APPLICATION OF ENSEMBLE MACHINE LEARNING TECHNIQUES IN CIVIL ENGINEERING MATERIALS

BY

IRWAN AFRIADI

A THESIS SUBMITTED IN PARTIAL FULFILLMENT OF THE REQUIREMENTS FOR THE DEGREE OF MASTER DEGREE OF CIVIL ENGINEERING
THAMMASAT SCHOOL OF ENGINEERING
THAMMASAT UNIVERSITY
ACADEMIC YEAR 2024

THAMMASAT UNIVERSITY
SCHOOL OF ENGINEERING

THESIS

BY

IRWAN AFRIADI

ENTITLED

APPLICATION OF ENSEMBLE MACHINE LEARNING TECHNIQUES IN CIVIL ENGINEERING MATERIALS

was approved as partial fulfillment of the requirements for
the degree of Master of Engineering (Thammasat School of Engineering)

on July 11, 2025

Chairman _____
(Associate Profesor Doctor Sayan Sirimontree)

Member and Advisor _____
(Associate Professor Doctor Chanachai Thongchom)

Member _____
(Associate Professor Doctor Suraparb Keawswasvong)

External Member _____
(Assistant Professor Doctor Penpichcha Sanit-In)

Dean _____
(Professor Doctor Sanya Mitaim)

Thesis Title	APPLICATION OF ENSEMBLE MACHINE LEARNING TECHNIQUES IN CIVIL ENGINEERING MATERIAL
Author	Irwan Afriadi
Degree	Master of Civil Engineering
Major Field/Faculty/University	Civil Engineering Thammasat School of Engineering Thammasat University
Thesis Advisor	Associate Professor Dr. Chanachai Thongchom
Academic Year	2024

ABSTRACT

The deterioration of reinforced concrete (RC) structures is primarily caused by the corrosion of steel reinforcement, significantly increasing maintenance and repair costs, while fire exposure further accelerates structural damage. Asa result, fiber-reinforced polymer (FRP) is a promising non-corrosive substitute for conventional steel reinforcement in RC construction. This study applies ensemble machine learning techniques, including XGBoost, AdaBoost, CatBoost, and Random Forest, to predict critical material properties in civil engineering. The models were used to estimate ultimate strength in FRP-concrete pull-out tests, ultimate shear stress at the FRP-steel interface, and residual steel strength properties post-fire exposure. In rank analysis, XGBoost is considered as the best technique in forecasting ultimate capacity of concrete-FRP pull-out test. In other hand, Adaboost is identified as the best-performing model in forecasting the ultimate shear capacity of FRP-steel test and steel residual post-fire mechanical properties test. Analysis of the feature importance revealed that the most influential parameters is bond length (l_b) for concrete-FRP pull-out test, CFRP thickness (t_C) for FRP-steel test, and temperature for post-fire steel properties. The findings highlight the effectiveness of machine learning in predicting material behavior.

Keywords: FRP, Machine Learning, Random Forest, XGBoost, CATBoost, ADABoost

ACKNOWLEDGEMENTS

In the name of the Almighty, the Most Merciful and Generous, Allah. I would like to thank my father and my dear mother for their unwavering support, love, and prayers. I also would like to thank Thammasat International Student Recruitment (TISR). Additionally, this work was supported by the Thailand Science Research and Innovation Fundamental Fund fiscal year 2024.

Thank you very much to my supervisor, Assoc. Prof. Dr. Chanachai Thongchom, for all of your help and patience in getting my thesis finished. I also want to thank all of my friends from the bottom of my heart. May Allah bless each and every one of you for always being an inspiration and motivator for me to accomplish my thesis.

Irwan Afriadi

TABLE OF CONTENTS

	Page
ABSTRACT	(1)
ACKNOWLEDGEMENTS	(3)
TABLE OF CONTENTS	(4)
LIST OF TABLES	(6)
LIST OF FIGURES	(7)
LIST OF ABBREVIATIONS	(8)
CHAPTER 1 INTRODUCTION	1
1.1 Background	1
1.2 Statement of Problem	3
1.3 Objective of Study	4
1.4 Objective of Study	4
1.5 Contributions	4
CHAPTER 2 REVIEW OF LITERATURE	5
2.1 Impact of Post-fire on Mechanical Properties of Steel Reinforcements	5
2.2 Bond Behavior of FRP Bar-to-Concrete Joint	6
2.3 Bond Behavior of FRP Sheet-to-Steel Joint	7
2.4 Machine Learning	8
CHAPTER 3 RESEARCH METHODOLOGY	17
3.1 Bond Behavior between FRP Bar and Concrete Pull-Out Test	17

3.2 Bond Behavior of the FRP Sheet–Steel Shear Interface Test 20
3.3 Steel Post-Fire Test 22
3.4 Ensemble Machine Learning 23
3.4.1. Random Forest 24
3.4.2. XGBoost 26
3.4.3. CatBoost 27
3.4.4. AdaBoost 29
3.5 Metric Performance 30
3.5.1 Mean Absolute Error (MAE) 30
3.5.2 R-Square Error (R2) 30
3.5.3 Root Mean Square Error (RMSE) 31
3.6 Rank Analysis 31
3.7 Sensitivity Analysis 31

CHAPTER 4 RESULT AND DISCUSSION 33

4.1 Collected Database of ML 33
4.2 Metric Performances 35
4.3 Rank Analysis 47
4.4 Sensitivity Analysis 49

CHAPTER 5 CONCLUSIONS AND RECOMMENDATIONS 54

5.1 Conclusions 54
5.2 Recommendations 55

REFERENCES 56

BIOGRAPHY 62

LIST OF TABLES

Tables	Page
2.1 Literature review.	12
4.1 Statistical descriptive parameters of the concrete-FRP pull-out test dataset.	33
4.2 Statistical descriptive parameters of the steel-FRP shear test dataset.	34
4.3 Statistical descriptive parameters of the post-fire steel dataset.	34
4.4 Metric performances of the concrete-FRP pull-out test datasets.	35
4.5 Metric performances of the steel-FRP shear test datasets.	36
4.6 Metric performances of the *fu,T/fu* ratio test datasets.	36
4.7 Metric performances of the *fy,T/fy* ratio test datasets.	37
4.8 Rank analysis of FRP-concrete pull-out test.	48
4.9 Rank analysis of FRP-steel shear test.	48
4.10 Rank analysis of *fu,T/fu* post-fire steel test.	49
4.11 Rank analysis of *fy,T/fy* post-fire steel test.	49

LIST OF FIGURES

Figures	Page
3.1 Pull-out test setup: (a) without loaded end (b) with loaded end (Nepomuceno et al., 2021; Shan et al., 2023).	18
3.2 Failure mechanisms at different stages (Zhou et al., 2022).	19
3.3 Types of failure modes (Zhou et al., 2023).	20
3.4 Testing set up.	21
3.5 Failure modes of FRP sheet-steel.	22
3.6 Flowchart of ML process.	24
3.7 Decision tree algorithm.	25
3.8 Random Forest algorithm flowchart.	25
3.9 XGBoost algorithm flowchart.	27
3.10 CatBoost algorithm flowchart.	28
3.11 Flowchart of the AdaBoost algorithm.	29
4.1 P_{max} scatter plot of concrete-FRP pull-out test.	39
4.2 P_{max} scatter plot of steel-FRP shear test.	40
4.3 The *fu,T/fu* scatter plot of post-fire steel test.	41
4.4 The *fy,T/fy* scatter plot of post-fire steel test.	43
4.5 Taylor diagram concrete-FRP of pull-out test.	44
4.6 Taylor diagram of steel-FRP shear test.	45
4.7 Taylor diagram of *fu,T/fu* on post-fire steel test.	46
4.8 Taylor diagram of *fy,T/fy* on post-fire steel test.	47
4.9 PCC of concrete-FRP pull-out test parameter.	50
4.10 PCC of steel-FRP shear test parameter.	51
4.11 PCC of steel post-fire test parameters (a) ultimate strength ratio and (b) yield strength ratio.	52
4.12 XGBoost FI of concrete-FRP pull-out test.	52
4.13 AdaBoost FI of the steel-FRP shear test.	53
4.14 AdaBoost FI of steel post-fire test.	53

LIST OF ABBREVIATIONS

Symbols/Abbreviations	Terms
AFRP	Aramid Fiber-Reinforced Polymers
ANN	Artificial Neural Network
b_C	FRP Width
BFRP	Basalt Fiber-Reinforced Polymers
CAM	Cosine Amplitude Method
COV	Covariance
CFRP	Carbon Fiber-Reinforced Polymers
CZMPs	Cohesive Zone Model Parameters
d_b	Diameter Bar
E_A	Adhesive Elastic Modulus
E_C	FRP Elastic Modulus
Ef	Elastic Modulus
EO	Equilibrium Optimizer
EVS	Explained Variance Score
f_A	*Adhesive Tensile Modulus*
f_C	FRP Tensile Strength
fc'	Concrete Strength
Ff	Tensile Strength Bar
FI	Feature Importance
fu,T/fu	Ultimate Strength Ratio
fy,T/fy	Yield Strength Ratio
FRP	Fiber-Reinforced Polymers
GBM	Gradient Boost Model
GFRP	Glass Fiber-Reinforced Polymers
GEP	Gene Expression Programming
GPR	Gaussian Process Regression
IAE	Integral Absolute Error

l_b	Embedded Length Bar
LGBM	Light Gradient Boost Model
LSVR	Least Square Support Vector Regression
LVDT	Linear Variable Differential Transformer
MAE	Mean Absolute Error
MAPE	Mean Absolute Percentage Error
ML	Machine Learning
MLR	Multiple Linear Regression
MNVM	Metaheuristic Neuron-Vector Machine
MRE	Mean Relative Error
NID	Neural Interpretation Diagram
PCC	Pearson Correlation Coefficient
P_{max}	Ultimate Load
R^2	Coefficient Of Determination
RBFNN	Radial Basis Function Neural Network
RBPNN	Resilient Back-Propagating Neural Network
RC	Reinforced Concrete
RCSWs	Reinforced Concrete Structural Walls
RF	Random Forest
RFE	Recursive Feature Elimination
RMSE	Root Mean Squared Error
RRSE	Root Relative Squared Error
RSE	Residual Error
SVM	Support Vector Machine
SVMR	Support Vector Machines Regression
t_A	Adhesive Thickness
t_C	FRP Thickness

CHAPTER 1
INTRODUCTION

1.1 Background

Civil buildings and infrastructures could be structurally unacceptable for a variety of reasons, such as deteriorating materials, shifting loads on the structure, problems in design, etc. The corrosion of reinforcing steel rods is the primary factor in the deterioration of reinforced concrete buildings and has a significant impact on maintenance and repair costs. Fire is one of the most damaging environmental conditions that a structure might face throughout its lifetime. Structures become less able to resist loads at high temperatures. Steel decreases in stiffness and durability when the temperature rises (Jacintho et al., 2012). The mechanical, thermal, and deformation properties of steel are factors that influence how it reacts to fire. Analyzing the temperature distribution throughout the steel cross sections is essential for determining the steel's strength after exposure to fire. Studies conducted between 1980 and 2012 revealed that 30 bridge collapses were mostly caused by fire, while 20 bridge failures during the same era were caused by seismic stresses. This finding emphasizes the need of investigating the effects of fire on structures (Lee et al., 2013).

One of the more appealing options for replacing the ordinary steel rods in RC construction to address the corroded steel issue is fiber-reinforced polymer (FRP) rods (Irshidat, 2020). The majority of FRPs in the marketplace are constructed of aramid, glass, carbon, or basalt (AFRP, GFRP, CFRP, BFRP). These compounds frequently have polymer matrix construct on thermosetting resins particularly vinyl ester or epoxy systems (Rolland et al., 2018). FRP can be easily shaped into bars, sheets, plates, and other shapes (Zhang et al., 2022).

Analyzing the FRP bonding behavior of FRP materials is an essential part of structural engineering construction, particularly in regard to enhancing the performance and longevity of civil infrastructure. The effective performance of FRP composites in improving the strength of concrete frameworks largely based on the bond performances with the substrate of material. The application of advanced technologies, particularly

machine learning (ML), is growing progressively more important in order to improve these bonding interactions and provide more profound insight.

ML helps assist engineers and researchers to gain a better understanding of the complex relationship typical of FRP compounds. ML methods provide a new and data-driven approach to studying the complex interaction between the material substrates and the FRP composites using computer algorithms. That is, ML tools are computer algorithms capable of learning the data from dataset and utilizing the data to make predictions or assess outcomes.

Zhang et al. (2022) employed ML techniques for FRP flexural durability prediction in RC beams strengthened and ML models made more precise predictions compared to empirical models. ML models are capable of learning pattern and relationships from experimental data, allowing for more accurate predictions. Additionally, ML models are capable of generalizing and do not suffer from the issue of overfitting.

Barkhordari and Jawdhari (2023) applied ML techniques in the prediction of FRP flexural durability in reinforced RC beams the length of plastic hinges of reinforced concrete structural walls within seismic engineering design and evaluation to accurately forecast the behavior of structures. ML models provide a high-fidelity simulation tool in the approximation of the strain, capacity, and curvature demands of RCSWs, which are crucial for structural assessment and guaranteeing safety and resilience.

FRP bars have two unfavorable side effects, i.e., brittle elastic failure and a lower elastic modulus than steel in the case of GFRP bars (Alam & Hussein, 2013). CFRP bars have an elasticity modulus that is comparable to that of steel bars. Apart from that, FRP rebars have different bond and surface properties compared to steel rebars. Hence, FRP-RC structures also have different than those of steel-reinforced structures.

36 RC cylinders with BFRP and 12 RC cylinders with GFRP rods direct pullout experiments were performed by other researchers (El Refai et al., 2015). The test parameters included the rod diameter, the rod embedment length in the concrete, and the material used for the FRP (glass and basalt). The bond-slip curves of the GFRP and

BFRP bars showed comparable tendencies. The rods made from BFRP had an average bonding strength that was 75% weaker than that of the rods made from GFRP.

Pull-out samples using GFRP rods with diameter of 12.7 mm exhibited marginally greater bonding strength outcomes than samples using deformed steel rods with diameter of 12 mm, which is very promising (Rolland et al., 2018). Pull-out tests were performed to find out the abilities of the CFRP, BFRP, and GFRP by placing the bar in recycled aggregate concrete and pulling them away from the concrete (Godat et al., 2021). The use of BFRP rods may enhance the postpeak bonding performance. These results suggest that the kind of bar may affect the bonding behavior.

1.2 Statement of Problem

Most material construction projects use steel constructions for a wide variety of building types, including huge industrial buildings, high-rise constructions, skyscrapers, and bridges, because of several advantages, including high strength, high ductility, lightweight, and easy design (Kumar et al., 2021). Steel exhibits outstanding strength at room temperature; nevertheless, as with other materials, when the temperature rises, steel loses stiffness and strength (Kodur et al., 2010). Understanding the impact of post-fire distribution is essential for analyzing the strength of steel.

Another construction material is FRP. One of the critical aspects of utilizing FRP composites effectively in structural construction is learning about their bonding behavior with different substrates, particularly concrete. The bond behavior of FRP materials is vital for confirming the structural strength and efficiency of FRP-strengthened structures.

At present, the use of FRP rods rather than steel rods to address corrosion-related issues is becoming increasingly popular. Nevertheless, FRP rebars have several disadvantages, including nonhomogeneous components, poor stiffness, and elastic linear performance, which lead to entirely variant mechanisms for the transmission of loads between rods and local concrete. Therefore, before adding FRP reinforcing bars to concrete buildings, it is vital to learn about the connection behavior of FRP rods and concrete (Irshidat, 2020).

In the present argument, authors are going to write the complex FRP bond behavior using machine learning, specifically for predicting the peak load (Pmax) of

different past experiments. ML model prediction accuracy has been discovered to be higher compared to empirical models (Zhang et al., 2022). In civil and structural engineering, ML is able to investigate the influencing factors on bonding performance and its importance. Engineers and researchers are able to make the right decisions, improve structural designs, and provide durability and safety for FRP, steel, and concrete construction by studying the behavior performances.

1.3 Objective of Study

The objectives of these studies are as follows:

1) To apply ensemble ML techniques to forecast the strength ratio of steel in experiment tests.
2) To apply ensemble machine learning models to forecast the bonding strength of the experimental FRP-steel interface pull-out tests.
3) To apply ensemble machine learning techniques to forecast the bonding strength of the experimental FRP-concrete interface tests.
4) The best model prediction from each prediction model was identified.

1.4 Objective of Study

1) This research study employs several ensemble models to forecast and compare the performance of each machine learning model.
2) The best performance is obtained from several evaluation methods, such as metric performance, the Taylor diagram, and ranking analysis.

1.5 Contributions

The primary benefit of the current thesis research is to investigate the efficacy of ML approaches with different combinations of input variables. The objective of this research thesis is to determine the ideal correlation between the data-driven system's input and output. By evaluating the prediction test accuracy, machine learning will demonstrate the best performance of the connection between the input and output datasets. The result will predict the best performance of machine learning to forecast the experimental tests for each test.

CHAPTER 2
REVIEW OF LITERATURE

2.1 Impact of Post-fire on Mechanical Properties of Steel Reinforcements

Since many buildings, such as nuclear reactors and chimneys, are subjected to prolonged high temperatures, research has been conducted to determine how reinforcing bars are affected by high-temperature conditions. Numerous aspects, including the steel form, manufacturing technique, chemical formula, exposure temperature, heating degree, heating method, cooling degree, cooling method, and surface features, influence the reinforcing steel performance of heated residual mechanical materials. The production method has a significant impact on the strength of reinforcing steel as the temperature rises (Tariq & Bhargava, 2018).

More sophisticated building materials have been created and used for steel construction, particularly large-space structures, long-span bridges, and super high-rise buildings. The steel structural systems used in buildings must adhere to the fire resistance requirements of building regulations since fire is one of the most severe situations that a structure may experience during its lifespan (Wang et al., 2013). Steel can tolerate temperatures as high as 500°C, but above that point, it tends to lose most of its strength and becomes easily damaged by fire (Chiew et al., 2014; Usmani et al., 2003).

Heat causes the mechanical properties of steel to degrade during fires, and the yield strength of ordinary steel at 600°C is less than 1/3 of the yield strength at room temperature (Ünlüoğlu et al., 2007). According to the literature, steel's yield strength and maximum strength decrease if the temperature increases, and the strength is insignificant at 580°C (Elghazouli et al., 2009; Felicetti et al., 2009). When the exposure time was increased to the same temperature, the yield strength and elongation changed dramatically, but the ultimate strength did not (Ahmad, 2017). Compared to conventional steel, high-strength steels are more unstable when heated (Maraveas et al., 2017). The previously stated fact suggests that when employing high-strength steel, fire design is an essential loading condition. The qualities of high-strength bolt steel were assessed and discovered that the chemical structure of the steel influences its

composition at post-fire. The tensile strength, yield strength, and elastic modulus significantly decrease as the temperature increases to 700°C, whereas the elongation of the steel increases (Li et al., 2003).

2.2 Bond Behavior of FRP Bar-to-Concrete Joint

The mechanics of bond stress transmission in concrete-FRP reinforcements have been extensively researched by many scholars. The impact of many factors, including cross-sectional shape, embedment length, and rebar type, was examined in the EUROCRETE project. Various FRP reinforcement forms of pull-out mechanisms that are now in use have been found to rely on even more factors and variety than deformed steel rods. The overall pattern showing decreased binding strengths for larger rebar diameters is evident throughout all the findings from earlier research (Baena et al., 2009).

Generally, FRP rods are composed of brittle polymers, have an elastic modulus that is lower than steel rods, are more easily accessible, and cost less than CFRP and AFRP bars (Başaran et al., 2022). For GFRP and BFRP rods, this is particularly relevant because the moduli of elasticity are only around a quarter (¼) to a fifth (⅕) of those of steel bars, ranging from 40 to 60 GPa. (Liang et al., 2023). Although AFRP bars are known to provide better mechanical attributes and long-term durability than GFRP and BFRP rods, they are pretty prone to UV effects. The greatest tensile and fatigue strengths, as well as being the most resilient FRP form to temperature, humidity, corrosion, fatigue, and creep rupture, are just a few of the advantages that CFRPs possess over the other three varieties. Yet, CFRP also has some drawback of significant importance, including its expensive nature, electrical conductivity, sensitivity to electrochemical degradation under wet conditions exposed to reaction with metal components, and brittleness. (Başaran et al., 2022).

Direct pull-out and beam bonding tests are the most widely employed techniques in deciding the bonding performance of FRP rebars with concrete. The simples of the two conduct is the direct pull-out test and it has been effectively utilized in previous studies examining the bonding capacity of FRP bars inserted in concrete according to available guidelines (Rolland et al., 2018).

Many variables, such as the bar diameter, embedment length of bar, concrete compressive strength, specimen surface shape, concrete cover, and bar position, affect the capability of bond behavior. Mathematical expressions were derived to predict the bonding strength of FRP bars in concrete, and various experiments were conducted to assess the effect of the variables on bond performance capability. Two of the principal parameters in the majority of formulas presented in literature were the rod diameter and the strength of concrete. Bar embedment location, bar type, concrete cover, surface treatment, and bar embedment length were not taken into consideraation (Saleh et al., 2019).

Bonding between FRP rods and standard concrete has been analyzed extensively. Most previous literatures have investigated a range of variables affect bonding of FRP with concrete. The FRP rods' bonding strength was dominated by their interlaminar strength and higher concrete strengths (Hossain et al., 2018). Moreover, it was determined that the bonding capacity of the FRP bars decreased with an increase in diameter. Moreover, the bonding strength ability of the FRP bars reduced with increase in bars embedded length. another article claimed the primary cause of bond strength is the mechanical surface interaction of bars (Peng et al., 2022).

2.3 Bond Behavior of FRP Sheet-to-Steel Joint

Several experimental studies have been performed to assess the interfacial performance of steel-FRP. Experimental tests usually use simple CFRP-steel bonded interactions, including beam double-shear and single-shear joints, because of their easy manufacturing and testing processes. Double-lap shear joint behaved mechanically in relation to six different steel surface treatments. The findings indicated that higher grit sizes produced higher ultimate loads and that grit blasting using a silane coupling agent outperformed grit blasting by approximately 12% of the maximum load (Ou et al., 2023). Single-lap shear testing of CFRP and steel bonding performance was employed to examine adhesive toughness and bonding thickness. The results demonstrated that a greater effective bond length was achieved because of the robust adhesive, greater maximum load, and lower stiffness of the CFRP-steel bonding than those of the brittle glue (Z. Wang et al., 2021).

A number of research works have examined the CFRP-steel bonding surface failure mechanisms. The failure mechanisms of CFRP or the type of epoxy glue used might affect CFRP-steel bonding surface failure mechanisms. Failure mechanisms of CFRPs and steel bonding are more complex and varied. Failure modes are divided into six types: FRP rupture, FRP delamination, adhesive and FRP interfacial bonding, steel and adhesive interfacial bonding, adhesive failure and steel yielding (Pang et al., 2020; Wu et al., 2012). The adhesion failure occurred with a greater modulus but delamination of CFRP was triggered by a linear adhesive with lower modulus (He & Xian, 2016). Thickness of the adhesive layer has significant influences on failure mechanism, bond-slip behavior, and maximum load capacity (Wang et al., 2016a).

2.4 Machine Learning

Machine learning models were employed to forecast the interfacial bonding strength of FRP-concrete composites (Zhang et al., 2023). The article constructs a big dataset of FRP-concrete direct shear test specimens and uses an unsupervised isolation forest to improve data quality. Six machine learning models are trained and compared, and the XGBoost model has the best prediction accuracy. A novel prediction equation for the bonding strength is derived in this work from the influencing factors that are used by machine learning techniques. From the experiment results, the machine learning models were found to perform better than the existing formula in the literature. This work is beneficial for the prediction of FRP–concrete bonding strength and offers an interpretable machine learning method for the same.

A study on the accuracy of the present models for forecasting the bonding strength of FRP and concrete. Zhou et al. (2020) collected significant quantities of experimental data comprised of 969 values of single-lap shear test results on FRP-concrete interfacial bonding and evaluated the predictive capability of various models. They found that most existing models do not have high precision due to the fact that various parameters are expressed with irregular expressions. They then used a neural network model to train and test data and developed a new explicit formula to predict bond strength. The new model was more precise compared to existing models. The authors concluded that the model could be used in engineering design.

Zhang and Xue (2021) introduced the development and comparison of two machine learning models, GEP and RF, to predict the bonding strength of FRP rods or sheets in concrete. The models were compared using statistical indicators and with available empirical models, and they showed higher accuracy and lower error values. The statistical indicators that were utilized in assessing the performance of the GEP and RF models were the MAE, R2, RMSE, MAPE, RRSE, and IAE. The most accurate model was the RF model, followed by the GEP, Seracino, and Zhang models. The GEP and RF models gave R2 values of 0.871 and 0.800, respectively, which suggests that the models can accurately and reliably predict bonding strength. Bond strength increased with the increasing bond length, groove depth-to-width ratio, FRP axial stiffness, and compressive strength of the concrete.

Kim et al. (2022) also introduced research on predicting the bonding strength of FRP-concrete composites with ensemble ML techniques. The performance metrics used in the research to evaluate the bond strength prediction model are RMSE, R2, COV, and IAE. The bonding strength of FRP-concrete composites depends on different parameters that comprise surface preparation, concrete quality, FRP stiffness, bond length, and adhesive properties. The CATBoost algorithm outperformed other ensemble algorithms, including XGBoost and random forest, in terms of many of the performance metrics like RMSE, R2, IAE, COV, EVS, MSE, MAE, and RE.

ML approaches were presented to accurately examine FRP and concrete interfacial cohesive parameters (Su, Peng, et al., 2021). The authors develop an artificial neural network (ANN) model that uses the load-displacement responses of a finite element model to predict the cohesive zone model parameters (CZMPs). The ANN approach is trained and tested with datasets composed of 130 load–displacement responses. The performance of the test showed that the mean absolute percentage errors (MAPEs) of the two parameters (interface shear strength and corresponding slip) were 2.941% and 2.078%, respectively. The ML model is able to predict well interface feature problems that either fall outside the training set or in the gap in the data, with best MAPEs under 3% and 4% for the two parameters.

ML methods, especially an RBPNN, to estimate the shear strength of FRP sheet externally joined reinforced concrete beams were utilized by Abuodeh et al. (2020). The researchers collected a database of 120 tested specimens and utilized the RBPNN

model coupled with the RFE method and NID method. The RFE algorithm was utilized to identify the dataset's most significant independent parameters. The input of the ANN model variables was understood and their values tracked visually by employing the NID. The result showed that the model involving all the default variables performed worse than the RBPNN with the specified parameters and already made standard predictions. The study found that one of the best methods for assessing FRP performance in shear–strengthened beams is through the employment of an RBPNN involving RFE and NID.

Basaran et al. (2021) investigated the bonding strength and FRP rod length evolution in concrete. Machine learning algorithms and code equations applied to estimate bond strength are also introduced in the paper. Machine learning techniques applied in the paper to estimate the bonding strength of FRP rods in concrete were GPR, ANN, SVMR, RT, and MLR. The accuracy of some methods and equations is compared, and the influence of several factors on bonding strength is evaluated. Four code equations were compared. These code equations include ACI 440.1R-15, CSA S806-12, JSCE-SF4, and fib Model Code 2010. The formula of ACI 440.1R-15 performed better since the code had the lowest error intervals and the best R2 score.

The prediction of interfacial bond strength of FRP-concrete composites was explored with machine learning techniques (Su, Zhong, et al., 2021). The research compares the performance of MLR, SVM, and ANN techniques on the basis of two datasets of experimental results, discusses the influences of the input parameters, and suggests a stacking strategy to improve the predictive accuracy. The SVM-ML approach yielded the highest R2 value and the lowest RMSE, MAE, and MRE values among the other algorithms. The SVM-ML approach also achieves better predictive accuracy compared to the existing empirical approaches. The study concluded that it is possible and effective to estimate the bonding strength of FRP-strengthened concrete structures through the use of machine learning approaches.

A novel model, MNVIM for predicting the bonding capacity of an FRP-concrete interface was introduced by Wang et al. (2022). The MNVIM combines the RBFNN and LSVR using an equilibrium optimizer (EO). The MNVIM model is more accurate than other artificial intelligence methods and mathematical methods in predicting bonding strength. In comparison to BPNN, RBFNN, SVR, and LSVR

traditional AI models, MNVIM generates significantly smaller values of MAPE, RMSE, and MAE. The MNVIM also performs better than ensemble LSVR + RBFNN with MAPE, RMSE, and MAE improvements of around 15.23%, 5.92%, and 5.06%, respectively. Compared to common mathematical techniques, the MNVIM generates smaller values of COV and RMSE, that is, better accuracy in prediction. MNVIM outperforms other models of artificial intelligence and mathematical approaches in prediction of bonding strength in concrete element repair/rehabilitation.

Bayesian optimization and machine learning-based data-driven strategies to determine the bond-slip interface model of the FRP-concrete contact were recommended by Yuan et al. (2022). Different machine learning models have been compared, and their hyperparameters have been tuned in order to further enhance the prediction accuracy. The machine learning models used in the research were linear regression, Bayesian ridge regression, LGBM, SVR, DT, model, XGBoost, GBM, CATBoost, and stacked regressor models. The proposed technique is confirmed by numerical simulations and experiment results. The paper also considers the hyperparameter optimization process, the generality and accuracy of the proposed model, and the bond behavior of different configurations of FRP sheets and concrete under different conditions of loading. The predictive validity of the proposed model, determined by measures such as R2 (coefficient of determination) and COV (coefficient of variation), was high. The R2 value was said to be 0.98, which indicates high dependence between the calculated and observed values. The COV was said to be 3.73%, indicating a low dispersion of prediction results. Overall, our Bayesian optimization with a Gaussian process facilitated a good and efficient search for optimal ML hyperparameter models, and our CATBoost regressor was better compared to other machine learning models based on the accuracy of prediction because it posted the lowest root mean square error (RMSE) amongst the tested models. The results of various studies are outlined in Table 2.1.

Table 2.1 Literature review.

Author	Research Topic	Objective	Variables	Model	Result
Zhou et al. (2020)	Explicit neural network model for predicting FRP-concrete interfacial bond strength based on a large database	This journal used a total of 20 existing models for predicting the bond strength of FRP-concrete tested utilizing single-lap shear test. These models were compared to the actual test results to assess their accuracy.	Pu (ultimate bond strength), fc' (concrete compressive strength), Kf (FRP stiffness), bf (FRP sheet width),-κw (width correction factor), and -κL (length influence coefficient).	ANN	Chen and Teng's model has the best accuracy.
Abuodeh et al. (2020)	Prediction of shear strength and behavior of RC beams strengthened with externally bonded FRP sheets using machine learning techniques	The results of this work may help researchers and structural engineers simulate the shear strength of reinforced concrete beams externally by using newly developed machine learning methods.	beam width (Bw), effective depth of beam (deff), shear span-to-depth ratio (a/d), compressive strength of concrete (fc), yielding strength of stirrups (fy, s), Area of stirrups-to-spacing ratio (Av/S), thickness of FRP sheet (tf), width of FRP U-wrap (Bf), height of FRP strip (Hf), transverse FRP strip width-to-spacing ratio (Wf/Sf), and FRP elastic modulus (Ef) and shear capacity.	RBPNN with NID and RFE machine tools	RBPNN model with selected features outperformed existing design standards, such as ACI, *fib*14, and CNR-DT200, in forecasting the FRP shear capacity of reinforced concrete beams

Table 2.1 Literature review (continued).

Author	Research Topic	Objective	Variables	Model	Result
Zhang and Xue (2021)	A predictive model for the bond strength of near-surface-mounted FRP bonded to concrete	To put out a novel empirical formula that uses the pull-out test to forecast the strength of the connection between FRP rods or sheets and concrete in the near-surface-mounted (NSM) method	Bond length (L), FRP axial rigidity (EfAf), groove depth-to-width ratio (Dg/Wg), epoxy tensile strength (fe), and concrete compressive strength (f'c)	GEP and RF	RF model had the best performance.
Su, Peng, et al. (2021)	Identification of the interfacial cohesive law parameters of FRP strips externally bonded to concrete using machine learning techniques	To show that, using the observed load–displacement response, the proposed machine learning approach can reliably detect the interfacial CZMPs of EB CFRP-to-concrete connections.	The applied load and the corresponding displacement at the interface between the FRP and concrete, Interface shear strength (CZMP1), Slip corresponding to the interface shear strength (CZMP2)	ANN	ANN model accurately identifies the parameters. MAPE for the two parameters, (CZMP1) and (CZMP2), are 2.941% and 2.078%, respectively.

Table 2.1 Literature review (continued).

Author	Research Topic	Objective	Variables	Model	Result

Basaran et al. (2021)	Estimation of the FRP-concrete bond strength with code formulations and machine learning algorithms.	The goal of this research is to use machine learning methods to create precise models for calculating the binding strength between FRP bars and concrete using four test methods (Hinged Beam Specimen (HBS), Beam End Specimen (EBS), Splice Specimen (SS) and Pull-out Specimen (PS) tests).	u (bond strength), db (diameter of bar), fc (compressive strength of concrete), C (concrete cover), L (embedment length of bar), A_{tr} (area of transverse bar), s (spacing of transverse bars), n (number of bar being developed along the plane of splitting).	ANN, SVMR, GPR, RT and MLR.	The most effective methods for forecasting the bond strengths were GPR and ANN.
Su, Zhong, et al. (2021)	Selected machine learning approaches for predicting the interfacial bond strength between FRPs and concrete.	Give an example of how to use the stacking technique to combine various ML algorithms in order to increase the prediction accuracy.	Interfacial bond strength(P_{exp}), Elastic modulus of the FRP plate (Ef), Tensile strength of the FRP plate (ff), Thickness of the FRP plate (tf), Width of the FRP plate (bf), Bond length between FRP and concrete (Lf), Compressive strength of the concrete (fc), Width of the groove (bg), Depth of the groove (hg).	MLR, SVM, and ANN.	The SVM was the best prediction accuracy among the three machine learning algorithms.

Table 2.1 Literature review (continued).

Author	Research Topic	Objective	Variables	Model	Result
Kim et al. (2022)	Ensemble Machine	The goal is to develop a bond strength prediction	bond strength (Pu), Concrete cube strength (Fc), Concrete cylinder	ANN, CATBoost,	The best performance

	Learning-Based Approach for Predicting of FRP–Concrete Interfacial Bonding.	model based on the ensemble approach, which will be trained using a sizable dataset of single-lap shear bond tests conducted on FRP–concrete specimens gathered from published research.	strength (Fc'), Concrete strength (Ft), Elastic modulus (Ef) of the FRP, Thickness of the FRP (tf), Width of the FRP (b), Thickness of the concrete material (t).	XGBoost, Histogram Gradient Boosting, and Random Forest.	achieved by the CatBoost algorithm.
Wang et al. (2022)	Smart ensemble machine learner with hyperparameter-free for predicting bond capacity of FRP-to-concrete interface: Multinational data.	The goal is to provide a reliable tool for predicting bonding strength to improve the safety and effectiveness of concrete structure repair and rehabilitation using FRP.	Concrete (compressive strength, tensile strength) and FRP (thickness of the FRP sheet, width of the FRP sheet, bond length of the FRP sheet, width of the concrete substrate).	MNVIM BPNN, RBFNN, SVR, LSVR, LSVR + RBFNN, EO-LSVR, and EO-RBFNN.	The MNVIM model achieves superior prediction performance compared to other models.

Table 2.1 Literature review (continued).

Author	Research Topic	Objective	Variables	Model	Result
Yuan et al. (2022)	Bayesian optimization for selecting efficient machine	This work suggested a strategy for using Bayesian optimization to the selection of effective	bond-slip relationship, elastic modulus of FRP, the elastic modulus of concrete, the bond	LR, BR, LGB, SV DT, RF	CatBoost regressor outperformed other machine learning

	learning regressors to determine bond-slip model of FRP-to-concrete interface.	machine learning models in order to ascertain the bond-slip response of the FRP-to-concrete interface through the use of test procedures for both single and double shear.	length, the bond width, and the concrete compressive strength.	XGBoost, Gradient boost, CATBoost, and Stacked Regressor.	models in accuracy prediction.
Zhang et al. (2023)	Prediction of FRP-concrete interfacial bond strength based on machine learning.	To Investigate 6 Machine Learning for predicting the FRP-concrete Interfacial bond Strength tested using single-lap or double-lap shear tests.	bond strenght (Pu), Concrete Tensile strength and compressive strength (ft & f'c), widths of the concrete block and fiber strip (bc & bf), and stiffness of the fiber strip (kf).	XGBoost, SVM, GBDT, DT, RF, and ANN.	XGBoost model had the best performance.

CHAPTER 3
RESEARCH METHODOLOGY

3.1 Bond Behavior between FRP Bar and Concrete Pull-Out Test

A pull-out test is an experiential test conducted to ascertain the bonding strength between the concrete-reinforcement rods. It involves applying a tensile force to a reinforcement bar that has been placed in concrete and measuring the amount of power required to pull the bar out from the concrete. The test provides valuable information about the bond behavior, including peak load, slip, and failure mode (Baena et al., 2009).

During the pull-out test, the reinforcing bar is typically inserted in a concrete specimen, and the load is gradually applied until failure or significant deformation. The force-displacement relation is determined, allowing for assessment of the maximum load and slip at maximum load. The pull-out test was conducted according to standardized procedures, e.g., as provided in standards (Chen et al., 2023).

The test rig involves the utilization of a test machine having load capacity and control of deformation, mounting the reinforcement bar on the grip system, and the measurement of slip using displacement transducers such as LVDTs. The test specimens are prepared with specified dimensions and surface finish, and tests are typically performed after a specified curing duration (Shan et al., 2023). Figure 3.1 illustrates the test setup for the pull-out test for diverse resources.

The results of the pull-out test provide valuable information for the comprehension of the reinforcement bar-concrete bond behavior and can be used to validate design guidelines and theoretical models. The results are compared based on the influences of the concrete strength (f_C'), elastic modulus (E_f), tensile strength bar (F_f), bar diameter (d_b), and bar embedded length (l_b). Based on different studies on bond behavior through pull-out tests, it is possible to conclude the following:

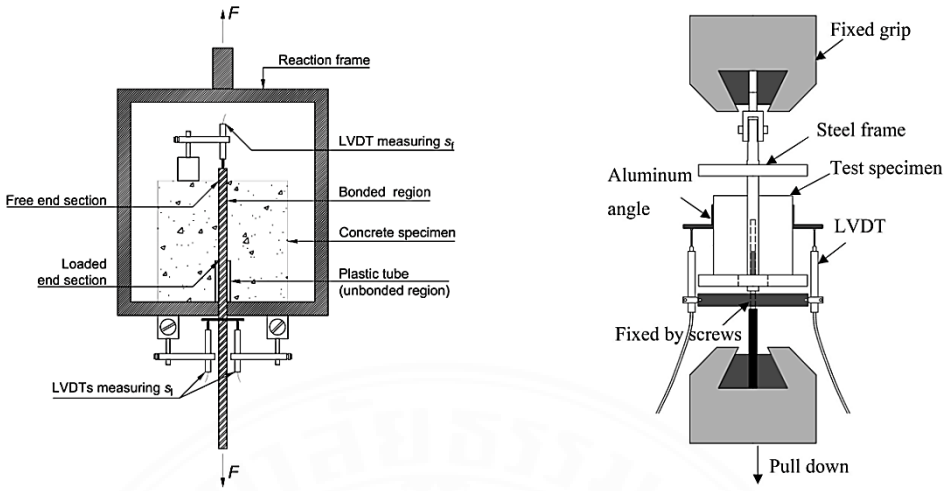

(a) (b)

Figure 3.1 Pull-out test setup: (a) without loaded end (b) with loaded end (Nepomuceno et al., 2021; Shan et al., 2023).

1. Maximum Bond stress

The stress distribution is not continuous along the embedment length in the pull-out test. Therefore, the following defines an average bond stress:

$$\tau_{max} = \frac{P_{max}}{\pi d_b l_b} \quad (1)$$

where d_b is the rebar diameter, l_b is the embedment length, and P_{max} is the maximum tensile load. The bond behavior is analyzed using the connection between the slip between the rebar and the concrete and the bond stress indicated by Eq. (1).

In this research, P_{max} is predicted using several variable parameters, namely, d_b, l_b, *fc'*, *Ef*, and *Ff*.

2. Bond stress–slip relationship

Four stages may be distinguished from conventional bond-slip curves: hardening, softening, descending, and residual phases. The load increased linearly throughout the early hardening stage. The adhesion between the two CFRPs and the concrete elements was the key factor in resisting the bond. After that, the stress increased nonlinearly until it reached its maximal value. Because of the reinforcements' ribs, the adhesion decreased at this time, and the mechanical interlock mostly resisted the connection. In the second phase, the slip continued to increase while the stress

remained at a specific amount. A tiny quantity of concrete was heaped by the rib as the loading operation proceeded. Small amounts of concrete were placed by the rib as the loading operation proceeded. The rigidity softened as a result of the mechanical interlock's reduced ability to resist force. The third stage revealed a significant reduction in stress when the depth of the concrete adequately restrained the CFRP bar. At this point, the interlock slowly disappeared with increasing stacking, providing resistance. Friction was the principal force resisting the connection. The process of full pull-out is shown in the fourth and final step. The residual friction was the only thing resisting the connection (Zhou et al., 2022). Figure 3.2 provides a thorough schematic picture that explains how the bond resistance for the four stages of loading develops.

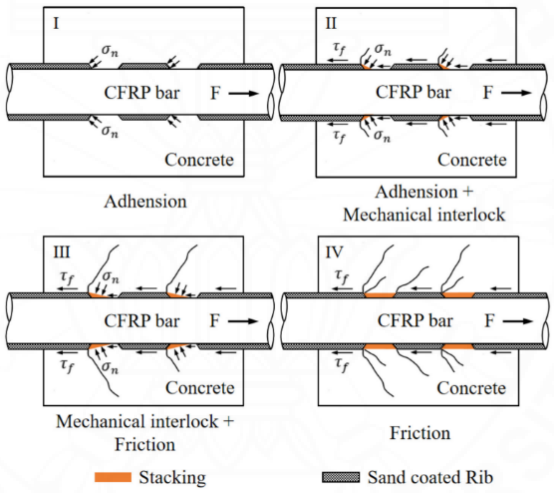

Figure 3.2 Failure mechanisms at different stages (Zhou et al., 2022).

There are two sides of the pull-out test in which the relative slip between the FRP and concrete can be measured by variable displacement transducer, Linear Variable Differential Transformer (LVDT), which are the loaded end and unloaded end. The loaded end is the side closest to the FRP bar that is loaded with a tensile load during the pull-out test. The unloaded/free end is opposite to the loaded end (Zhou et al., 2022).

3. Failure modes

There are several types of failure modes in the pull-out test: splitting failure, pull-out failure, and feeling-off/broken bar failure. Splitting failure occurred when a concrete experiment cracked into two or more pieces. The tensile failure of the section

referring to the examined bar appeared to be the cause of the splitting failure. as shown in Figure 3.3 (a). Pull-out failure occurs whenever the link between the concrete and rod breaks, causing the sample of concrete to collapse, as shown in Figure 3.3 (b). A feeling-off/broken bar occurred when the rib height of the rod strongly decreased because the coated sand particles were completely eliminated, as shown in Figure 3.3 (c) (Zhou et al., 2023).

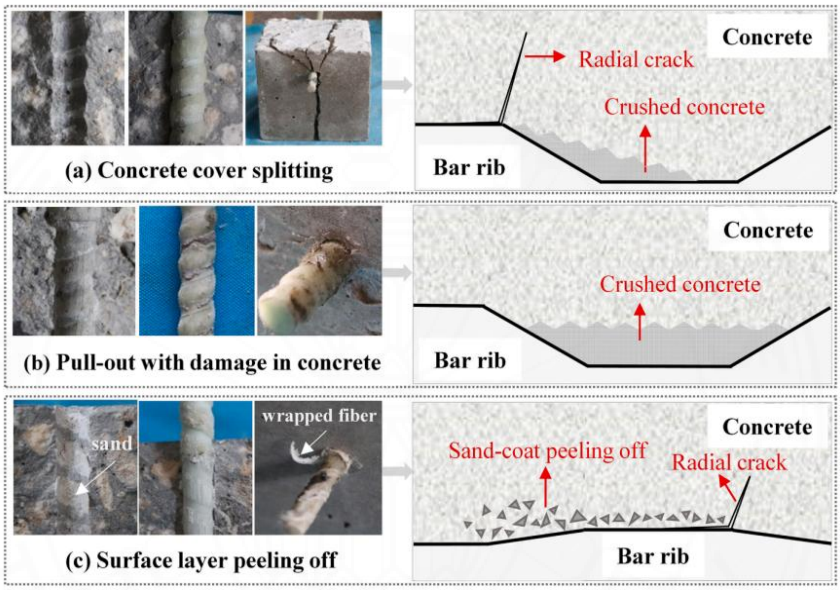

Figure 3.3 Types of failure modes (Zhou et al., 2023).

3.2 Bond Behavior of the FRP Sheet–Steel Shear Interface Test

In the field of structural engineering, shear joints play a crucial role in providing the necessary strength and stability for various structures. Shear joints refer to the connections between two structural elements designed to transfer shear forces (Zhao & Zhang, 2007). These kinds of joints find their use in various applications like construction of buildings, bridges, and equipment in industry. It is required to specifically define and check the characteristics of such shear joints to impart them safety and reliability (Sundarraja & Rajamohan, 2009). Single-lap and double-lap shear joints are two of the most popular shear joints. A single-lap shear joint is a type of joint where two structural members are overlapped and bonded to one another to create a joint (Samad et al., 2016). The joint is most often taken up in adhesions at the FRP and steel interface. Single-lap herein refers to FRP glued together with adhesive to a single

steel. Double-lap shear joints, nonetheless, involve bonding and overlapping two other structural members with a larger overlap length than single-lap joints. In this case, double-lap is FRP bonded with adhesive on two steels which are with gap. The test procedures show valuable information about the conditions of bonding in addition to the performance of the shear joint, including its strength, durability, and fatigue life. Figure 3.4 (a) and (b) show the outcome of single shear and double shear tests.

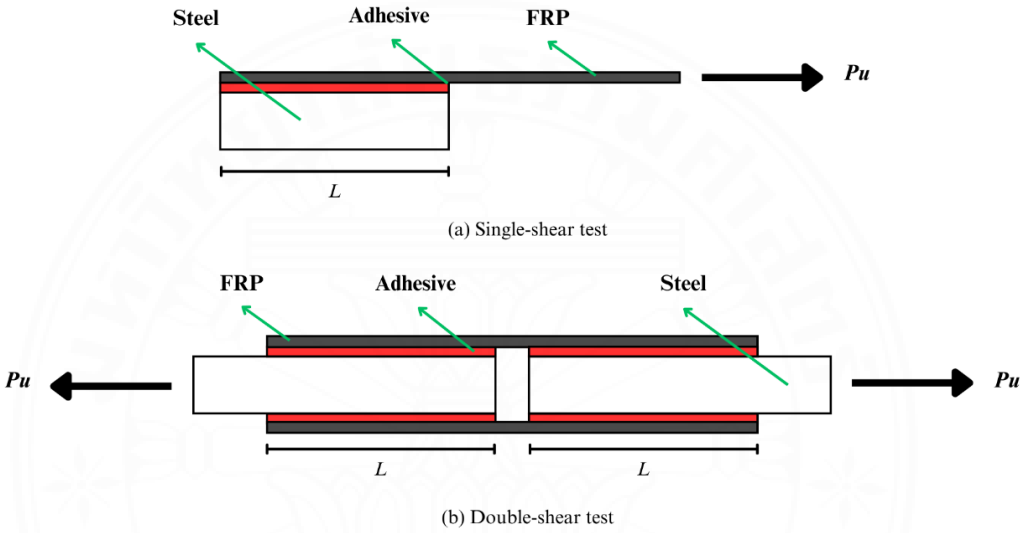

Figure 3.4 Testing set up.

The results of the shear interface test of FRP-steel are a valuable source of information in understanding steel-FRP sheet bond and can act as a verification tool for theoretical models and design guidelines. The results are analyzed based on the influence of the FRP elastic modulus (E_C), FRP width (b_C), FRP tensile strength (f_C), FRP thickness (t_C), adhesive thickness (t_A), adhesive elastic modulus (E_A), adhesive tensile modulus (f_A), bond length (L_C), and ultimate load (P_{max}). Based on a number of bond behavior studies in the context of interface shear tests, the following may be concluded:

1. Bond-slip relationship

The connection between the relative slippage of the FRP laminate of the steel substrate and the shear stress is known as the bond-slip relationship. Models of FRP-steel bonds are derived in large part from the bond-slip connection. It is capable of

accurately forecasting the FRP-steel bond's mechanical behavior (Z. Wang et al., 2021). The trapezoidal and triangular bond-slip models may be utilized to explain the FRP steel bond-slip relationship based on data from the literature. The two forms differ because of the kind of adhesive material used; bilinear bond-slip shapes have been recorded for linear adhesive (brittle) material, whereas trilinear bond-slip shapes are produced by nonlinear adhesive (ductile) material (Altaee et al., 2022). The bond-slip characteristic of the FRP sheet-to-steel surface bond is strongly influenced by the mechanical characteristics and adhesive thickness (Fernando, 2010; Wang & Wu, 2018; Wang et al., 2016a, 2016b).

2. Failure modes

A crucial result of the experiment is the failure pattern of the FRP–steel shear contact, which provides more insight into load distribution. The following categories often describe the failure mechanisms of FRP-bonded steel components under tensile stress: adhesive failure, interfacial bonding of the FRP and steel, FRP rupture, FRP delamination, and steel yielding (H.-T. Wang et al., 2021; Yu et al., 2012; Zhao & Zhang, 2007). These failure modes are provided in Figure 3.5.

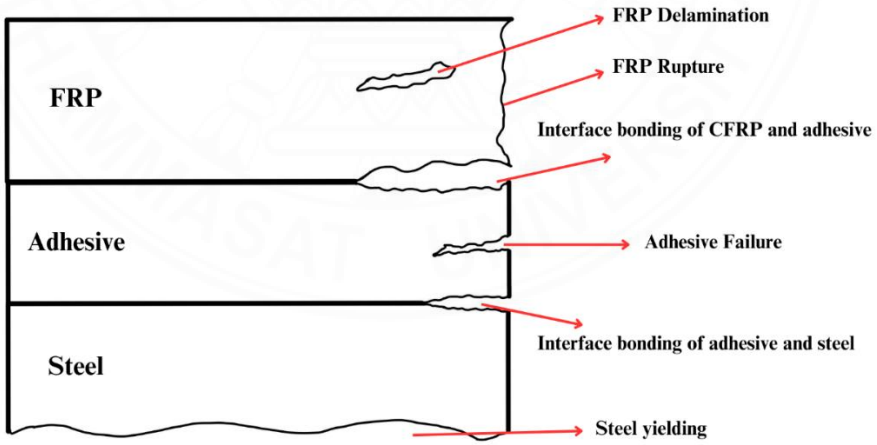

Figure 3.5 Failure modes of FRP sheet-steel.

3.3 Steel Post-Fire Test

In this section, the effect of post-fire on the steel performance is investigated. Many researchers have conducted experiments on steel post-fire tests. Stainless steel

post-fire was tested ranging from 100°C-900°C and subjected to heating rates ranging from 30 min to 60 min at intervals of 30 min in a fire furnace (Fan et al., 2016). Carbon steel post-fire was tested based on EN 1002-1 (En, 2001) at either 400°C or 700°C for various durations (Sulayman & Mahmood, 2021). The heating rate duration of the fire furnace ranged from 30 min to 120 min. Steady-state and transient-state tests were conducted (Chen et al., 2006). The heating rate of the steady-state test was less than 6°C (±3°C), and that of the transient-state test ranged from 100°C to 1000°C at intervals of 100°C. Quenched and tempered high-strength steel was tested (Wang et al., 2020). The fire furnace heating rates ranged from 100°C-1200°C, the heat soaking times ranged from 30 min to 240 min, and the cooling methods were used.

The steel samples were examined to get the ratio of the steel's post-fire mechanical properties and room temperature, which are the ultimate strength ratio ($f_{u,T}/f_u$) and the yield strength ratio ($f_{y,T}/f_y$). The steels were heated in a temperature-controlled furnace. The furnace heat temperature was set from normal room temperature until the target temperature was reached. Steel thickness (mm) and temperature (°C) are applied to analyze the steel's mechanical properties ratio.

3.4 Ensemble Machine Learning

Machine learning applications, which allow computers to learn from experience to solve structural material challenges, have been growing in the last few years. Supervised machine learning—in which the model is taught by applying inputs and outcomes—was recommended. Supervised machine learning methods can be divided into two types: regression and classification. Random forest regression, XGBoost, CATBoost, and ADABoost are adopted regression algorithms. In the field of structural materials and engineering, machine learning algorithms have been used to predict the compressive strength of concrete, detect and classify concrete cracks, classify the failure mode of beam-column joints, predict the shear strength, predict the behavior of beams reinforced with fiber-reinforced polymer (FRP) sheets, predict shear forces, and predict the FRP laminate–concrete bond (Chen et al., 2023). Flowcharts of ML processes are shown in Figure 3.6.

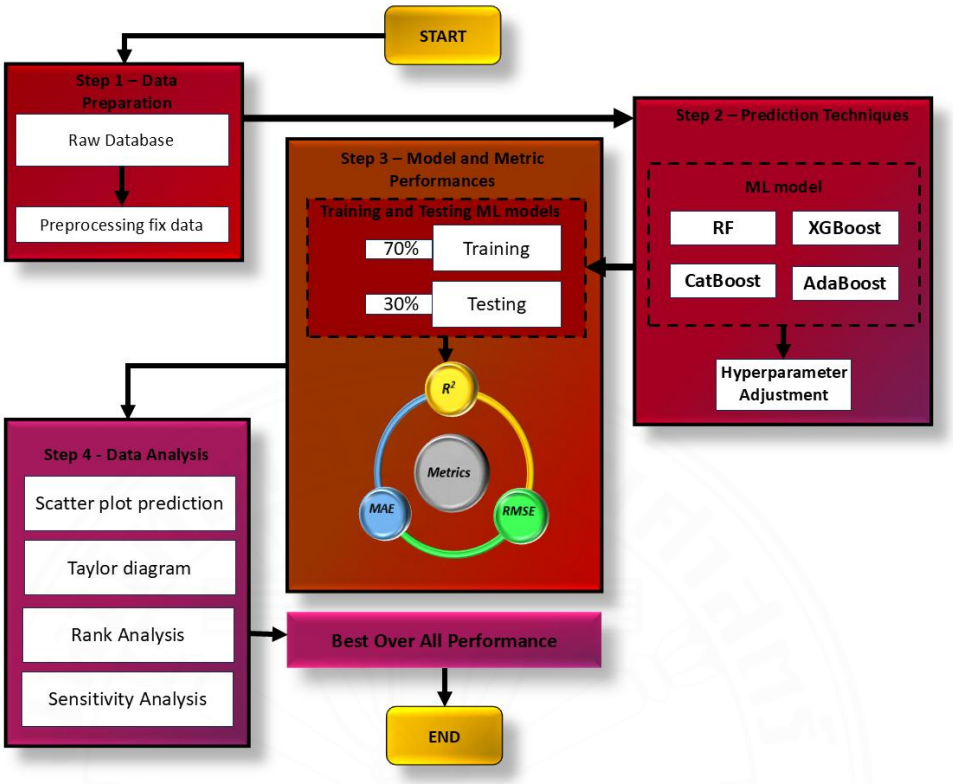

Figure 3.6 Flowchart of ML process.

3.4.1. Random Forest

Breiman (2001) initially presented the random forest (RF) technique in. It is a widely used approach that builds a sequence of decision trees for classification and regression. An ensemble technique for regression and classification is called a random forest (Zhang & Xue, 2021). By using the randomized feature, the RF technique decreases the correlation between the subtrees that are created. RF delivers a range of forest trees using bootstrap sampling. A distinct set of training data from the original dataset is used to train each decision tree in the forest. Every tree is given an additional diversity boost by RF as it develops (Kim et al., 2022). Bootstrapping refers to the resampling technique used to create multiple decision trees with different datasets, which are then combined to make predictions. Based on earlier research and surveys, it has emerged as the most often used ensemble approach because of its simplicity and effectiveness. Several steps for developing an RF model were proposed (Zhang & Xue, 2021). The first sample set must be created first, together with the crucial parameters and the variables that must be forecasted. Second, it is necessary to create multiple

regression trees (Ntrees). Decision and leaf nodes make up every decision tree that divides the original sample set into smaller subsets; the decision node has branches, but the leaf nodes stop splitting the data at that point, as shown in Figure 3.7. Next, in this procedure, how many randomly selected candidate variables (Mtry) are randomly selected at each node should be established. The best strategy for node splitting is chosen based on the minimum square error criterion, and the Mtry value is left constant. The decision nodes are divided up to the last leaf nodes. Figure 3.8 illustrates the Random Forest algorithm flowchart.

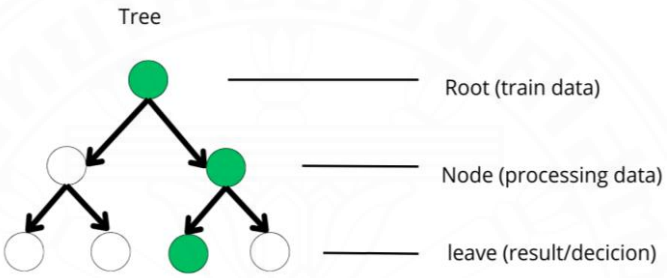

Figure 3.7 Decision tree algorithm.

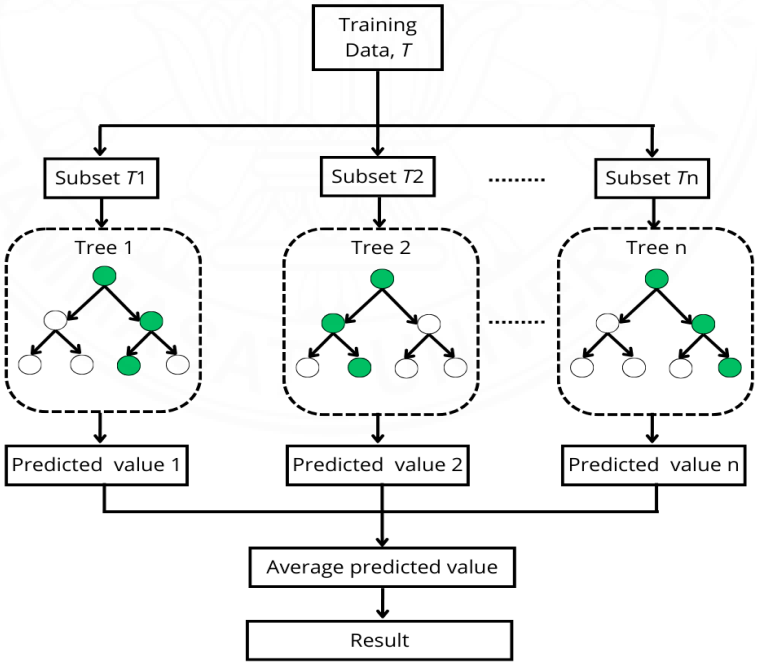

Figure 3.8 Random Forest algorithm flowchart.

3.4.2. XGBoost

The gradient boosting technique (XGBoost) is a popular and powerful machine learning method. According to (Kim et al., 2022), the XGBoost system is intended to be a precise and reliable tree boosting method. The features of XGBoost include reformulating the goal problem and adding regularization expression, sparsity awareness of the split function, approximated crack results based on one-sided quantile draws, and simultaneous tree learning utilizing column block cache awareness. XGBoost rapidly accelerates learning to its maximum by improving processing and memory capacity. A regularized model formulation is XGBoost's primary defense against overfitting, although it contains adjustments to lessen overfitting and other forms of extended problems. It also contains additional regularization methods, including instance subsampling and shrinking.

The data are compressed into columns and stored as memory blocks to increase accuracy. Each column is scanned linearly to obtain the split value. In the gradient statistics collection, the split values are combined and applied to every leaf in a single scan. This leads to the split value being determined by a parallel method. The splitting approach uses gradient values to access noncontiguous memory, which causes several instances of cache data to be missing. This issue is resolved by XGBoost by prebuffering and processing the necessary data. Figure 3.9 illustrates the XGBoost algorithm flowchart.

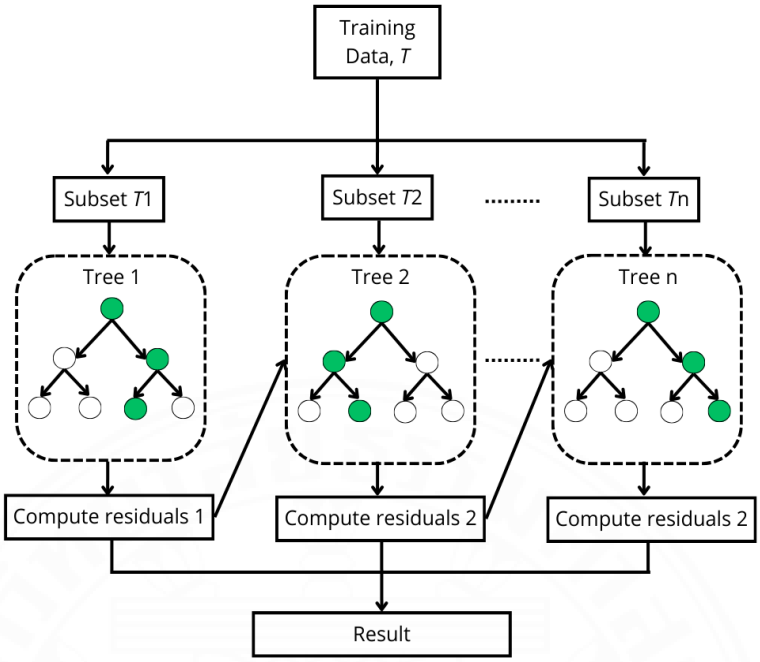

Figure 3.9 XGBoost algorithm flowchart.

3.4.3. CatBoost

CatBoost is a gradient boosting technique created especially to efficiently handle features with categories (Huang et al., 2019). CatBoost enhances performance and accuracy by accelerating the category feature process during tree splitting. Additionally, CatBoost presents minimal variance sampling (MVS), a method that aids in regularizing boosting models. Comparing MVS to other gradient boosting techniques, fewer examples are required for each boosting iteration, resulting in a higher-quality model. CatBoost also builds trees using symmetric trees, which allows for quicker results than other ensemble techniques. The method provides flexibility and adaptation for various modeling scenarios by offering a range of hyperparameters for customization and custom callback functions (Kim et al., 2022).

CatBoost has several features for prediction, namely, gradient boosting, ordered boosting, and feature importance. Gradient boosting works by combining a number of simple models (weak learners) sequentially. Each model is generated by minimizing the gradient of the loss function based on the residual error from the previous model. Ordered boosting provides special handling of categorical features. Ordered boosting helps improve the performance of datasets with categorical features and overcomes the manual encoding problem generally required in traditional boosting algorithms. The

feature importance functions assist in automatic feature selection. Feature importance can identify features that have an important influence on making accurate predictions and eliminate features that have a low influence.

Target statistics is a very effective technique for managing categorical characteristics with the least amount of information loss. A new feature might be created by combining all of the category features. In CatBoost, the combinations are considered a greedy method while creating a new split for the tree. For the first split in the tree, no combination is taken into consideration; however, CatBoost mixes all predefined combinations with all of the dataset's categorical variables for the second and subsequent divides. Every split that has been chosen in the tree is utilized in combination and is regarded as a category with two values. Figure 3.10 illustrates the CatBoost algorithm flowchart.

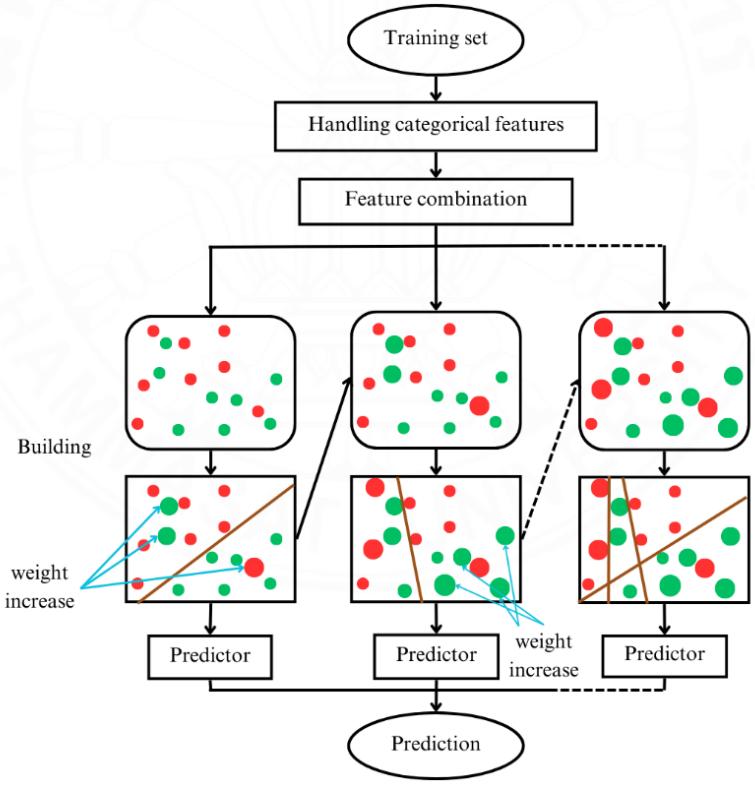

Figure 3.10 CatBoost algorithm flowchart.

3.4.4. AdaBoost

AdaBoost is an iterative boosting technique designed to enhance minority class categorization. The AdaBoost algorithm first assigns each observation to a variant weight. The weights assigned to the incorrectly categorized observations will increase after a few rounds, yet the weights of the correctly identified observations will decrease. The weights assigned to the observations serve as markers of the class to which the observation belongs, which reduces the misclassification of the observations and significantly enhances the performance of the classifiers (Rahman et al., 2015).

The AdaBoost algorithm is an ensemble learning technique that modifies the sample weight distribution to increase the accuracy of weak learners. The AdaBoost algorithm's computing phases for multiclassification issues are as follows: (1) For iteration step 1 (t=1), initialize the sample weights (w), w(x)= 1/N, where N is the number of examples. (2) Utilizing weights (wt), determine the optimal weak classifier (ht). (3) Determine the error rate (εt). (4) In the final hypothesis, provide weight ($wt+1$) to the classifier (ht); nevertheless, this step increases the weight above 100% or 1. (5) Normalize the weights so that $w(xi)$ = 1 is the maximum outcome (M12). Figure 3.11 illustrates the AdaBoost algorithm flowchart.

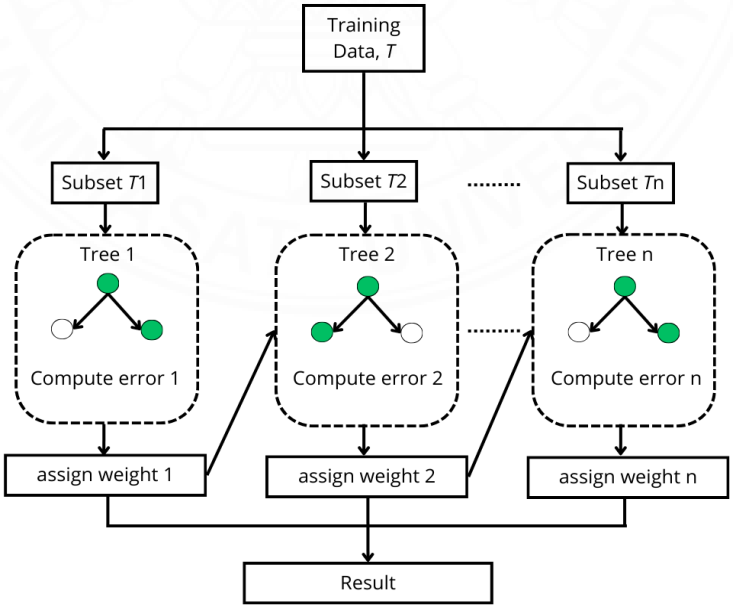

Figure 3.11 Flowchart of the AdaBoost algorithm.

3.5 Metric Performance

An ensemble method-based bonding strength prediction technique was constructed using a large number of test data from the literature. From the literature, test data examples were taken into examination. Each instance had input data and output data. There were 30% occurrences of the test data in the validation dataset compared to 70% instances in the training dataset. Three metric performance metrics were used to analyze the overall performance of the proposed ensemble methods: mean absolute error (MAE), R-square error (R^2), and root mean square error (RMSE).

3.5.1 Mean Absolute Error (MAE)

One of the evaluation measures used for evaluating how far a model's projected values deviate from actual values is the mean absolute error (MAE). The mean absolute error (MAE) is determined by averaging the absolute values of the deviations between the expected and actual values. The fundamental metric for evaluating mistakes is the MAE, which may immediately differ between the actual and predicted values. A model that performs better is indicated by a lower MAE. Equation 3.1 shows the formula for determining the MAE:

$$MAE = \frac{\sum_{i=1}^{n} |yi - \hat{y}i|}{n} \tag{3.1}$$

where yi is the predicted output value, n is the number of instances, and $\hat{y}i$ is the actual value.

3.5.2 R-Square Error (R^2)

The connection between the input and outcomes is measured by the R-square. The R^2, as it is called, analyzes the observation surrounding the fitted regression line. A value of R^2 closer to 1, which ranges from 0 to 1, indicates a significant correlation between the actual and anticipated values. Equation 3.2 shows the formula for determining R-square error:

$$R^2 = 1 - \frac{\sum i\,(yi - \hat{y}i)^2}{\sum i\,(yi - \underline{y}i)^2} \tag{3.2}$$

where $\underline{yi}$ is the average of the yi values, $\hat{y}i$ is the predicted value of yi, and y is the actual value.

3.5.3 Root Mean Square Error (RMSE)

The residual function standard deviation is known as the RMSE, which can reflect the errors between the actual and predicted values directly. It is a measurement of the error's average scale. By using Equation 3.3 to calculate the expected and actual observation values, the RMSE is determined:

$$RMSE = \sqrt{\frac{1}{n}\sum_{j=1}^{n}(yi - \hat{y}i)} \tag{3.3}$$

where yi is the predicted output value, n is the number of instances, and $\hat{y}i$ is the actual value.

3.6 Rank Analysis

Rank analysis is a way of measuring model performance. The model produces scores from performance measures that are totaled during testing and training. For a particular category, the higher the score, the better the prediction, and the lower the score, the more indeterminate. The model with the highest total score is ranked first, and the model with the lowest total score is ranked last. The suggested predictive ability models can be determined with the use of this procedure.

A Taylor diagram was used to analyze and compare the performance of each proposed model on the training and test datasets. Graphical comparison is used to quantify the effective implementation of machine learning models. This technique was formulated by Taylor (2001) for demonstrating and comparing the capability of various machine learning techniques.

3.7 Sensitivity Analysis

A technique of determining the value of each distinct input variable to the total output variance of a system is performing a sensitivity analysis. Sensitivity analysis is an effective tool for pinpointing the behavior of models and systems with respect to input variance. Sensitivity analysis tests systematically the interaction of input and

outcomes, which could help with decision alternatives, model accuracy, intervention, and research limitation. Post-training analysis, i.e., feature importance (FI) analysis, is a means of interpreting the results of ML models (Rengasamy et al., 2022). FI approximates each input feature (independent parameter) contribution to the output outcome (Arrieta et al., 2020). It is easier to explain actual cause and effect between significant data attributes and leads to models' inference in case FI is used to learn decision-making processes.

Another technique, the Pearson Correlation Coefficient (PCC), for identifying the correlation between two parameters, input to input or input to output, is also applied. The PCC measures the relationship between two parameters on a scale ranging from -1 to 1. A positive value represents a linear relationship between two variables. In contrast, a negative value represents a nonlinear relationship between two variables. The closer the PCC is to -1 or 1, the more powerful the relationship between variables. Equation 3.4 provides the PCC (r) mathematical expression.

$$r = \frac{\sum(M - \bar{M})(N - \bar{N})}{\sqrt{\sum(M - \bar{M})^2 \sum(N - \bar{N})^2}} \tag{3.4}$$

where $\bar{M}$ and $\bar{N}$ are the average values of two variables. M and N are the actual values of the two variables being examined.

CHAPTER 4
RESULT AND DISCUSSION

4.1 Collected Database of ML

4.1.1. Dataset of concrete-FRP pull-out test

1101 approach datasets have been collected from previous investigation tests. The datasets are divided into 70% for the training phase and 30% for the testing dataset. The following five input variables were included in the dataset for the present investigation i.e., modulus elastic (*Ef*), tensile bar (*Ff*), diameter bar (d_b), bar embedment length (l_b), concrete compressive strength (*fc'*), and one outcome variable, the ultimate load (P_{max}). The ranges of l_b and d_b are 3.3 mm to 21.25 mm, 9.53 mm to 285 mm, 35.74 GPa to 200 GPa for *Ef*, 540 MPa to 2800 MPa for *Ff*, 20.67 MPa to 114.34 MPa for *fc'*, and 3.11 kN to 121.79 kN for P_{max}. The statistical descriptive parameters of the concrete-FRP pull-out test dataset are summarized in Table 4.1. These datasets are split into 30% of the testing datasets and 70% of the training datasets.

Table 4.1 Statistical descriptive parameters of the concrete-FRP pull-out test dataset.

Statistics	d_b	l_b	E_f	f_f	f_c'	P_{max}
Minimum	9.53	3.3	35.74	540	20.67	3.11
Maximum	285	21.25	200	2800	114.34	121.79
Mean	62.65	11.06	68.21	1290.92	46.90	37.26
Standard Error	1.01	0.09	1.10	15.03	0.78	0.62
Median	50	10.1	50.67	1100	36.114	33.437
Mode	50	12	44	1100	27.768	26.03
Standard Deviation	33.49	3.02	36.46	498.84	25.75	20.73
Sample Variance	1121.78	9.09	1329.06	248841.22	662.95	429.70
Kurtosis	15.16	1.01	0.43	0.30	0.36	0.50
Skewness	3.29	0.51	1.42	1.13	1.24	0.88

4.1.2. Dataset of steel-FRP shear test

Numerous approaches have been proposed to assess the FRP-steel interfacial bond's performance, including single and double shear tests. In order to conduct this study, 317 prior experimental datasets of CFRP-to-steel bonded interfaces were used. These datasets included eight input parameters and one output parameter, which were the adhesive elastic modulus (E_A), adhesive tensile modulus (f_A), adhesive thickness (t_A), CFRP width (b_C), bond length (L_C), CFRP tensile strength (f_C), The CFRP elastic

modulus (E_C), CFRP thickness (t_C) and ultimate load (P_{max}). For small datasets, dividing the training and testing data into 30% and 70% is a common strategy. The input parameters E_A, f_A, t_A, E_C, f_C, t_C, b_C, L_C, and P_{max} have minimum and maximum values ranging from 1.46 GPa to 12.9 GPa, 15.10 MPa to 52.81 MPa, 0.15 mm to 3.16 mm, 155 GPa to 2861 GPa, 203 MPa to 3596 MPa, 0.17 mm to 1.50 mm, 10 mm to 60 mm, 10 mm to 435 mm, and 0.96 kN to 274.95 kN, in that order. Table 4.2 contains more statistical information about the steel-FRP shear test datasets.

Table 4.2 Statistical descriptive parameters of the steel-FRP shear test dataset.

Statistics	E_A	f_A	t_A	E_C	f_C	t_C	b_C	L_C	P_{max}
Max	12.90	52.81	3.16	2861	3596	1.50	60	435	274.95
Min	1.46	15.10	0.15	155	203	0.17	10	10	0.96
Mean	5.57	30.94	0.80	395.82	2356.45	1.27	36.64	165.82	56.06
Std. Dev.	4.01	7.24	0.46	628.40	855.66	0.37	14.35	112.16	38.51
Std. Error	0.22	0.41	0.03	35.29	48.06	0.02	0.81	6.30	2.16
Sample Variance	16.04	52.42	0.21	394891.9	732158.5	0.13	205.82	12578.76	1483.37
Skewness	0.64	0.75	1.31	2.97	-1.32	-2.63	-0.40	0.62	2.41

4.1.3. Dataset of post-fire steel test

A total of 274 datasets from post-fire material testing methods are used in publications addressing steel samples, which are split into 7:3 testing and training stages. The Four following factors were analyzed. Two factors, temperature (°C) and diameter (mm), are considered as input and two factors, yield strength ratio (*fy,T/fy*) and ultimate strength ratio (*fu,T/fu*), are considered as output. These parameters combined the mechanical and geometrical qualities of steel. The temperature applies from 25°C to 950°C, the steel's thickness ranges from 6 mm to 20 mm, and its ultimate strength ratio (*fu,T/fu*) is between 0.05 and 1.06. The yield strength ratio (*fy,T/fy*) is between 0.04 and 1,27. Table 4.3 contains more statistical information about the post-fire steel test datasets.

Table 4.3 Statistical descriptive parameters of the post-fire steel dataset.

Statistics	Diameter	Temperature	*fy,T/fy*	*fu,T/fu*
Max	25.00	950.00	1.27	1.06
Min	6.00	20.00	0.04	0.05
Mean	13.59	439.12	0.83	0.84
Std. dev	5.23	254.14	0.25	0.23
Std. error	0.32	15.35	0.01	0.01

Sample variance	27.34	64589.37	0.06	0.05
Skewness	0.82	0.03	-1.33	-1.81

4.2 Metric Performances

This section presents a comparative analysis conducted to evaluate the efficacy of four distinct models proposed: RF, XGBoost, ADABoost, and CATBoost. The metric performances for each test are presented in Tables 4.4 to 4.7. The metric performances of the ML algorithms in predicting the concrete-FRP pull-out test are displayed in Table 4.4. With an R^2 value of 0.99997, XGBoost became the best model for prediction during the training phase, according to a comparison of the performances of several metrics derived from various ML techniques. The second-best models were derived from the RF model in training phase, with an R^2 value of 0.99996; the third and fourth-best models in training phase were CatBoost and AdaBoost, with R^2 values of 0.9999 and 0.9995, respectively. In contrast, AdaBoost had the best prediction performance during the testing phase, with an R^2 value of 0.9994; second and third places in testing phase went to XGBoost and RF, with R2 values of 0.9993 and 0.9991, respectively. The last place in testing phase went to CatBoost with an R^2 value of 0.9957.

Table 4.4 Metric performances of the concrete-FRP pull-out test datasets.

ML model	Set	R^2	RMSE	MAE
AdaBoost	Train	0.9995	0.0038	0.0009
	Test	0.9994	0.0044	0.0011
CatBoost	Train	0.9999	0.0021	0.0016
	Test	0.9957	0.0119	0.0065
XGBoost	Train	0.99997	0.0009	0.0006
	Test	0.9993	0.0049	0.0016
RF	Train	0.99996	0.0012	0.0003
	Test	0.9991	0.0056	0.0010

The metric performances of the ML algorithms in predicting the steel-FRP shear test are displayed in Table 4.5. With a R^2 value of 1, AdaBoost became the best model for prediction during the training phase, according to a comparison of the performances of several metrics derived from various ML techniques. The second-best models were derived from the XGBoost model, with an R^2 value of 0.999997; the third and fourth-best models were CatBoost and RF, with R^2 values of 0.999984 and 0.998787,

respectively. For the testing phase, Adaboost still became the best model with a R^2 value of 0.998824. On the other hand, XGBoost became the second-best model followed by AdaBoost and RF with R^2 values of 0.998583, 0.998824, and 0.998555.

Table 4.5 Metric performances of the steel-FRP shear test datasets.

ML model	Set	R^2	RMSE	MAE
CatBoost	Train	0.999984	0.001965	0.001570
	Test	0.988705	0.050112	0.027530
AdaBoost	Train	1	0	0
	Test	0.998824	0.018344	0.006760
XGBoost	Train	0.999997	0.001044	0.000530
	Test	0.998583	0.018973	0.007230
RF	Train	0.998787	0.019318	0.045333
	Test	0.998555	0.017658	0.041023

The metric performances of the ML algorithms in predicting the *fu,T/fu* ratio of post-fire steel test are displayed in Table 4.6. With a R^2 value of 1, AdaBoost became the best model for prediction during the training phase, according to a comparison of the performances of several metrics derived from various ML techniques. The second-best models were derived from the XGBoost model, with an R^2 value of 0.99999; the third and fourth-best models were CatBoost and RF, with R^2 values of 0.99998 and 0.99977, respectively. For the testing phase, XGBoost becomes the best model with a R^2 value of 0.99910. AdaBoost becomes the second-best model followed by CatBoost and RF with R^2 values of 0.99860, 0.98255, and 0.96171.

Table 4.6 Metric performances of the *fu,T/fu* ratio test datasets.

ML model	Set	R^2	RMSE	MAE
CatBoost	Train	0.99998	0.0010	0.0008
	Test	0.98255	0.0315	0.0165
AdaBoost	Train	1	0	0
	Test	0.99860	0.0089	0.0045
XGBoost	Train	0.99999	0.0005	0.0003
	Test	0.99910	0.0117	0.0062
RF	Train	0.99977	0.0034	0.0013
	Test	0.96171	0.0477	0.0187

The metric performances of the ML algorithms in predicting the *fy,T/fy* ratio of post-fire steel test are displayed in Table 4.7. With a R^2 value of 1, AdaBoost became the best model for prediction during the training phase, according to a comparison of the performances of several metrics derived from various ML techniques. The second-best models were derived from the XGBoost model, with an R^2 value of 0.99999; the third and fourth-best models were CatBoost and RF, with R^2 values of 0.99995 and 0.99982, respectively. For the testing phase, XGBoost becomes the best model with a R^2 value of 0.99797. AdaBoost becomes the second-best model followed by RF and CatBoost with R^2 values of 0.99745, 0.99735, and 0.98435.

Table 4.7 Metric performances of the *fy,T/fy* ratio test datasets.

ML model	Set	R^2	RMSE	MAE
CatBoost	Train	0.99995	0.00170	0.00135
	Test	0.98435	0.03293	0.01931
AdaBoost	Train	1	0	0
	Test	0.99745	0.01333	0.00473
XGBoost	Train	0.99999	0.00057	0.00032
	Test	0.99797	0.01404	0.00701
RF	Train	0.99983	0.00325	0.00143
	Test	0.99735	0.01341	0.00492

4.2.1. Scatter plot

In this part, the measured and predicted output components are plotted on a scatter plot diagram, with the line y = x representing perfect alignment. Predictions that are closer to this line (x = y) suggest a more precise model and a point directly on the line indicates an ideal prediction. Figures 4.1 to 4.4 present the training and testing datasets of the scatter plot diagram of the concrete-FRP pull-out test, steel-FRP shear test, and post-fire test of steel on predicting *fu,T/fu* and *fy,T/fy* that the estimator outputs from AdaBoost methods are less scattered around the x = y line, leading to more refined results. Specifically, AdaBoost is able to focus on improving outcomes in challenging areas by assigning greater weight to previously misclassified instances and handling overfitting in small datasets. Taylor diagram of ML for each test is presented on the Figures 4.5 to 4.8.

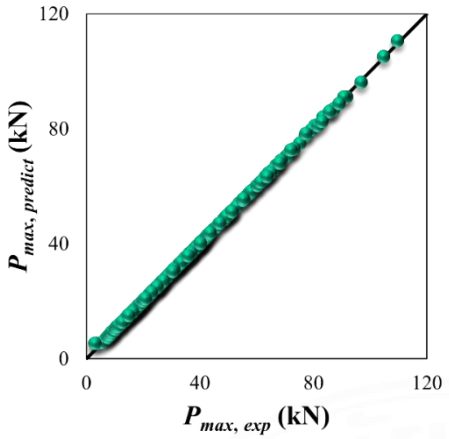

(a) AdaBoost testing phase.

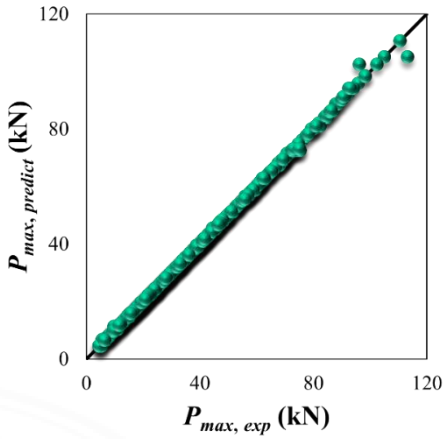

(b) AdaBoost training.

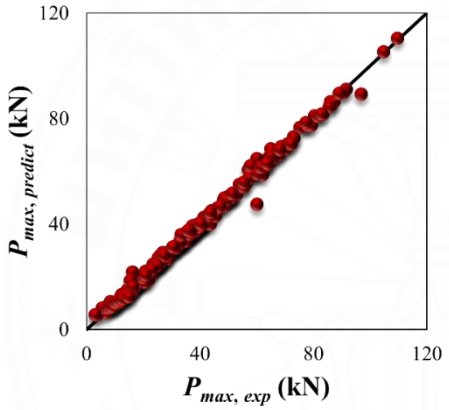

(c) CatBoost testing phase.

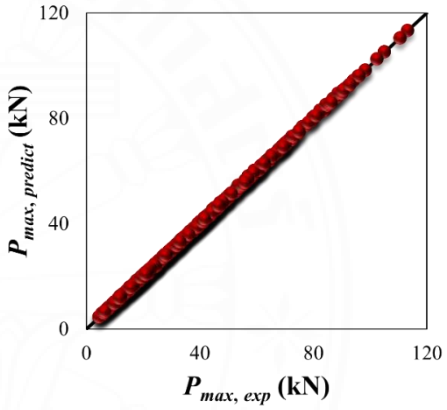

(d) CatBoost training phase.

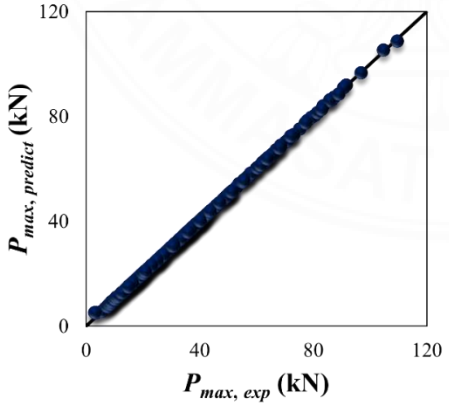

(e) RF testing phase.

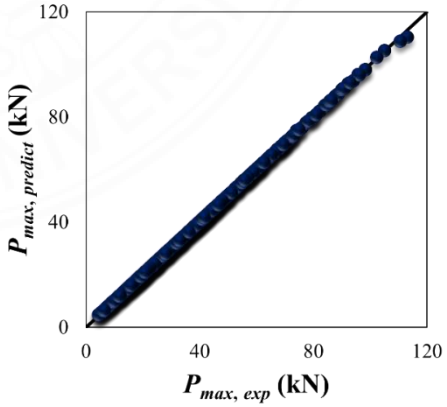

(f) RF training phase.

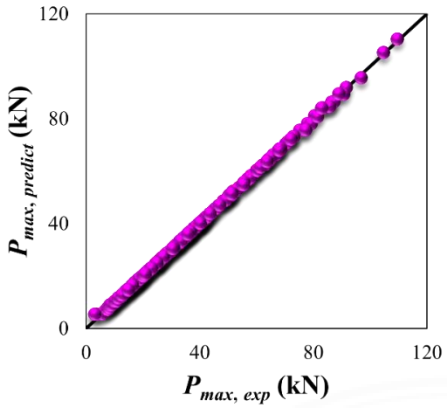

(g) XGBoost testing phase.

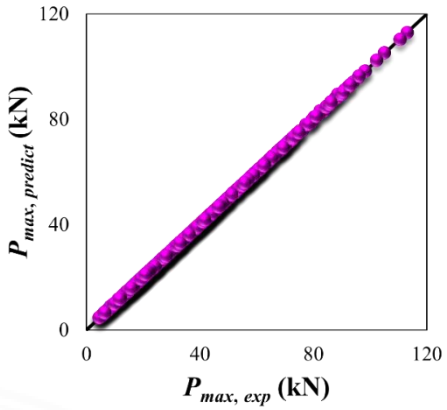

(h) XGBoost training phase.

Figure 4.1 P_{max} scatter plot of concrete-FRP pull-out test.

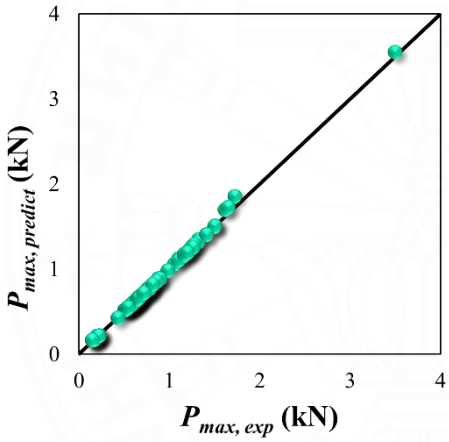

(a) AdaBoost testing phase.

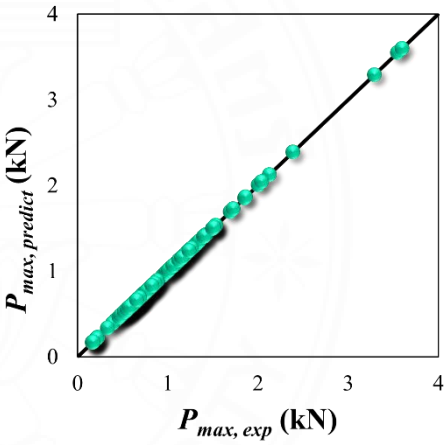

(b) AdaBoost training phase.

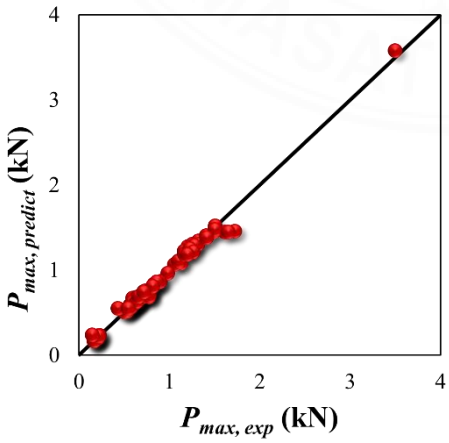

(c) CatBoost testing phase.

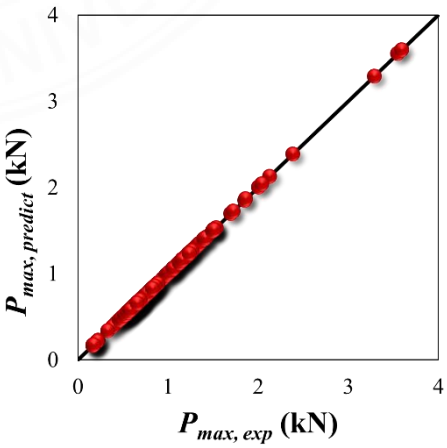

(d) CatBoost training phase.

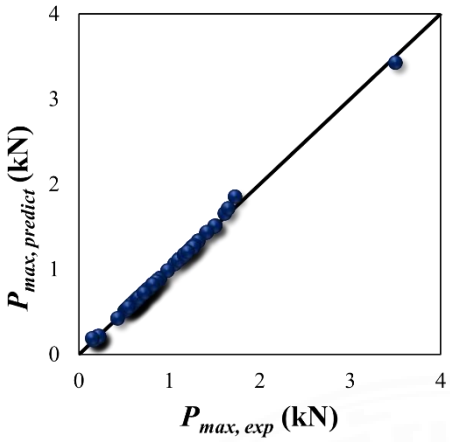

(e) RF testing phase.

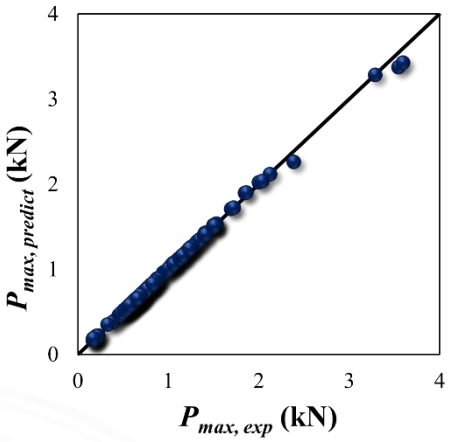

(f) RF training phase.

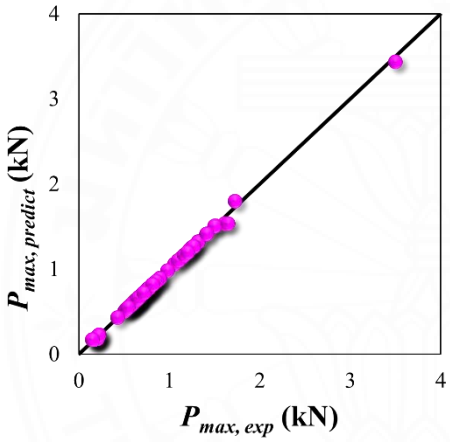

(g) XGBoost testing phase.

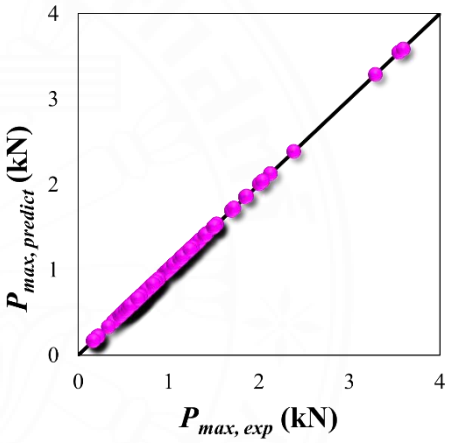

(h) XGBoost training phase.

Figure 4.2 P_{max} scatter plot of steel-FRP shear test.

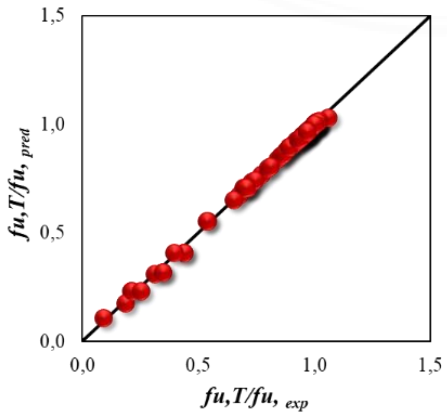

(a) AdaBoost testing phase.

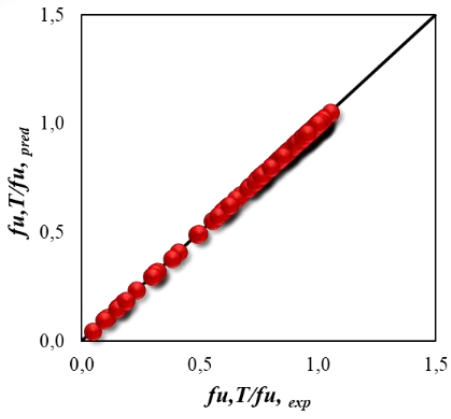

(b) AdaBoost training phase.

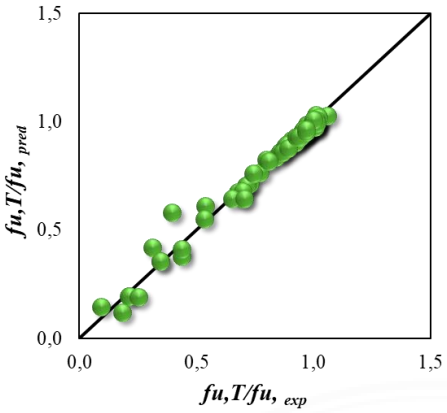

(c) CatBoost testing phase.

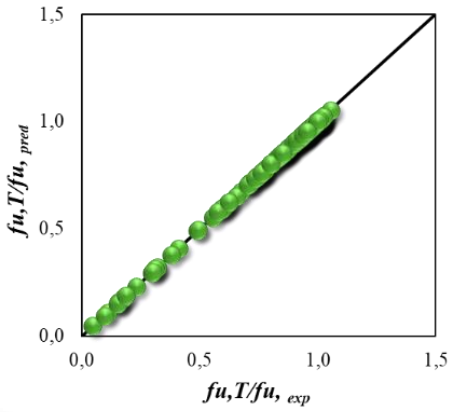

(d) CatBoost training phase.

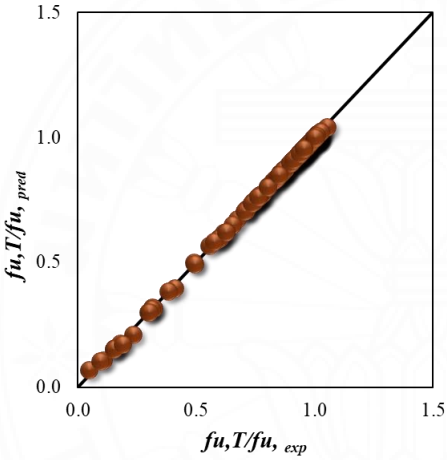

(e) RF testing phase.

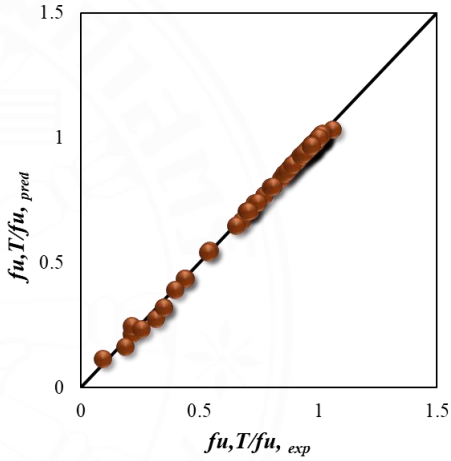

(f) RF training phase.

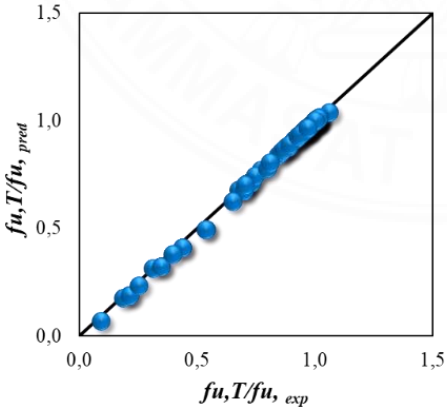

(g) XGBoost testing phase.

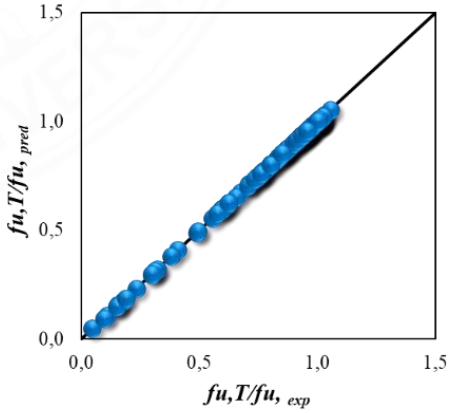

(h) XGBoost training phase.

Figure 4.3 The *fu,T/fu* scatter plot of post-fire steel test.

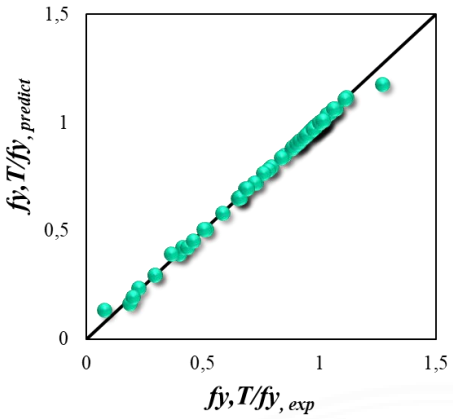

(a) AdaBoost testing phase.

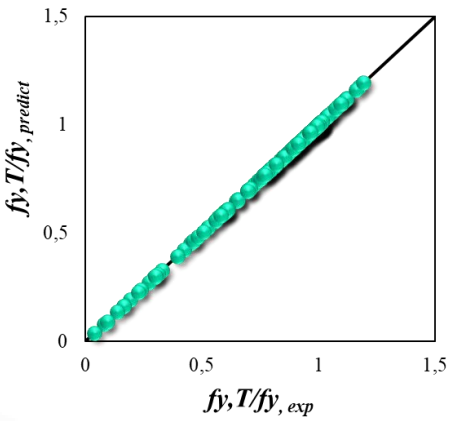

(b) AdaBoost training phase.

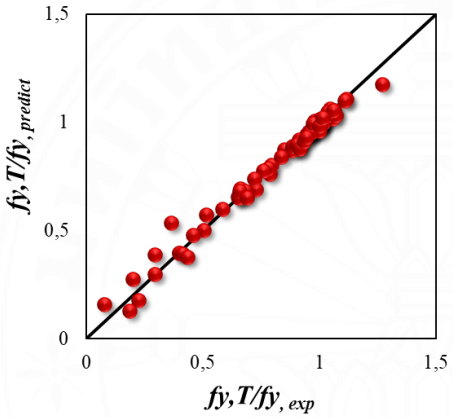

(c) CatBoost testing phase.

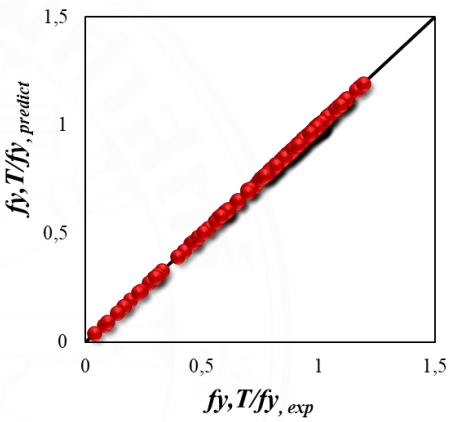

(d) CatBoost training phase.

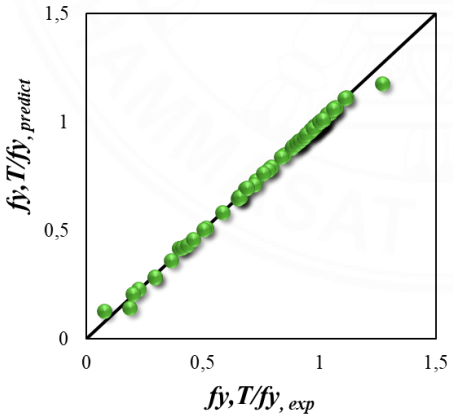

(e) RF testing phase.

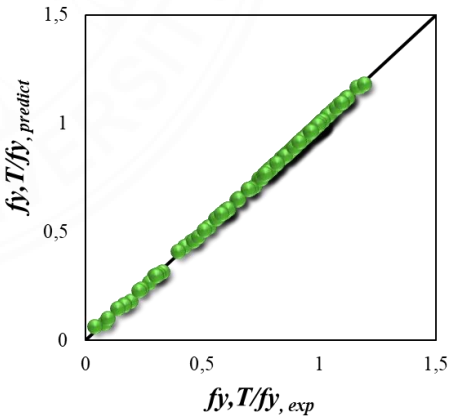

(f) RF training phase.

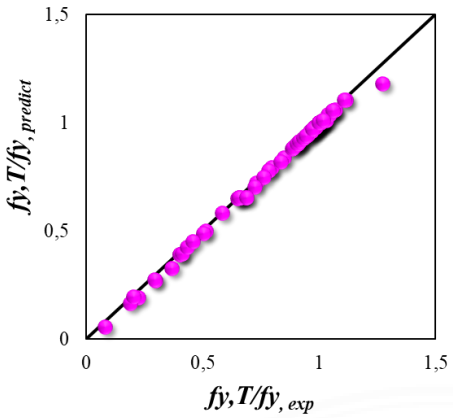

(g) XGBoost testing phase.

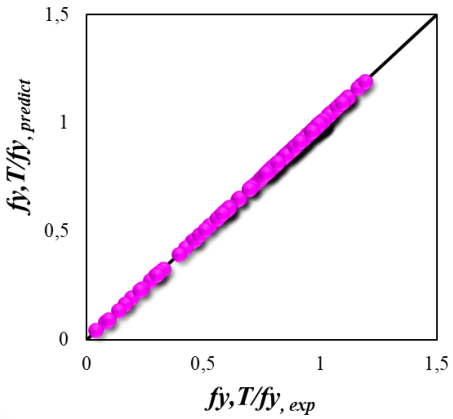

(h) XGBoost training phase.

Figure 4.4 The *fy,T/fy* scatter plot of post-fire steel test.

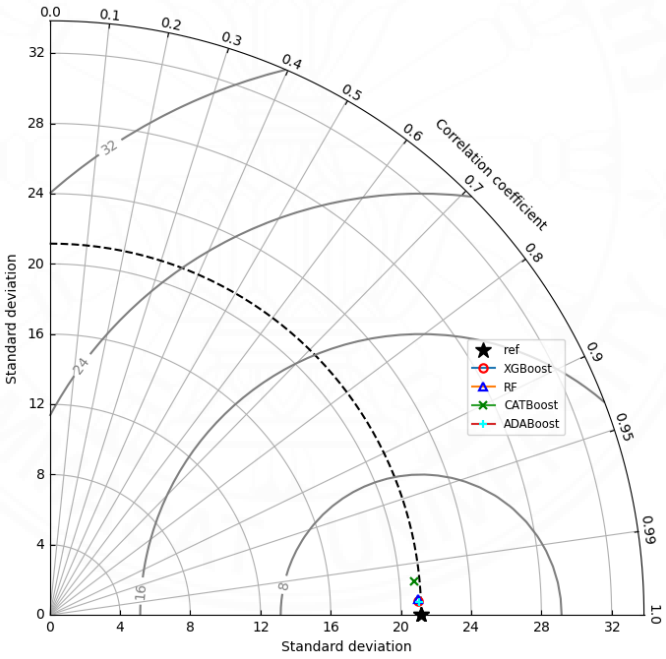

(a) Testing phase

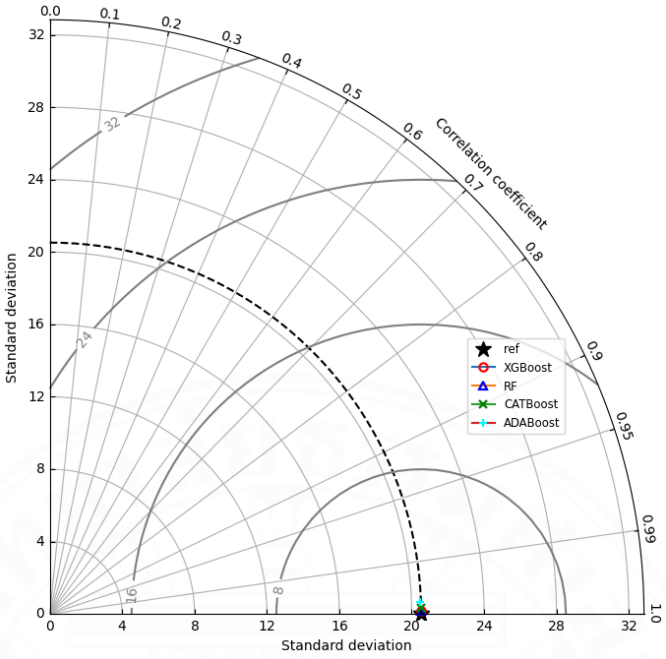

(b) Training phase

Figure 4.5 Taylor diagram concrete-FRP of pull-out test.

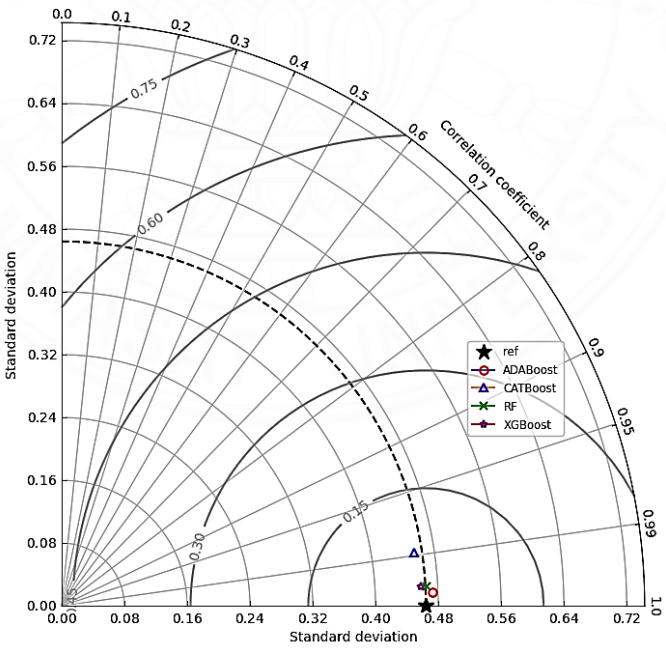

(a) Testing phase.

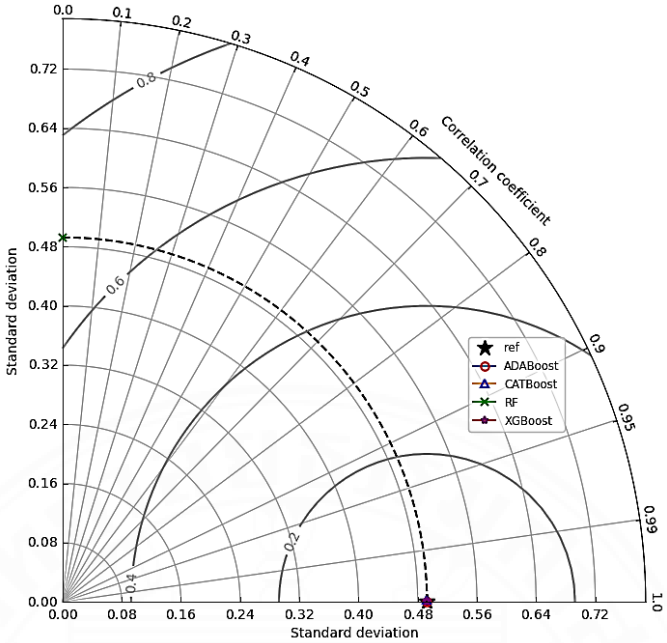

(b) Training Phase.

Figure 4.6 Taylor diagram of steel-FRP shear test.

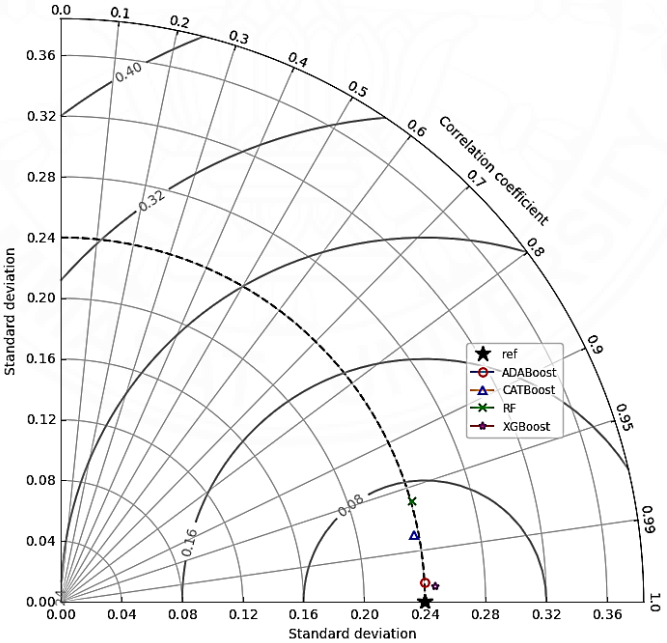

(a) Testing phase.

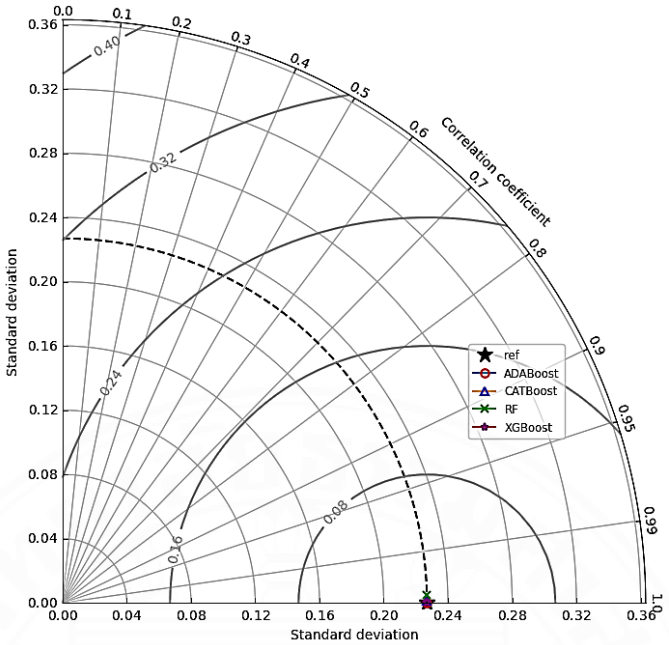

(b) Training phase.

Figure 4.7 Taylor diagram of *fu,T/fu* on post-fire steel test.

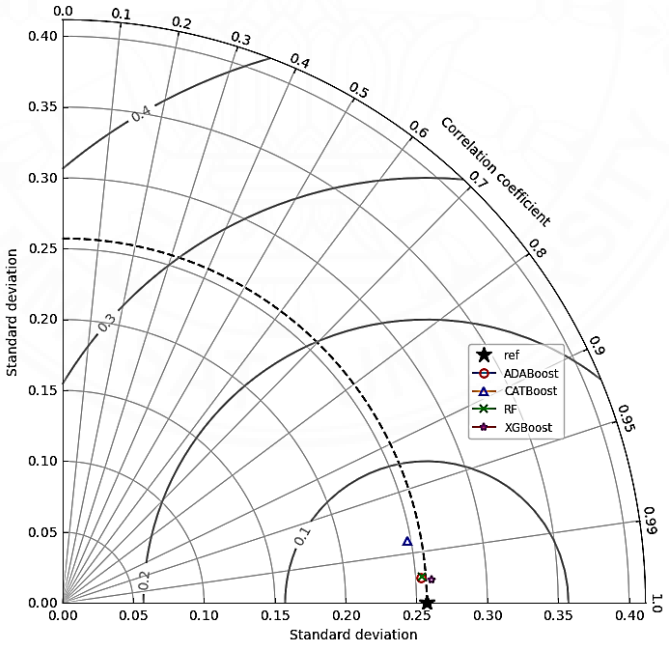

(a) Testing phase.

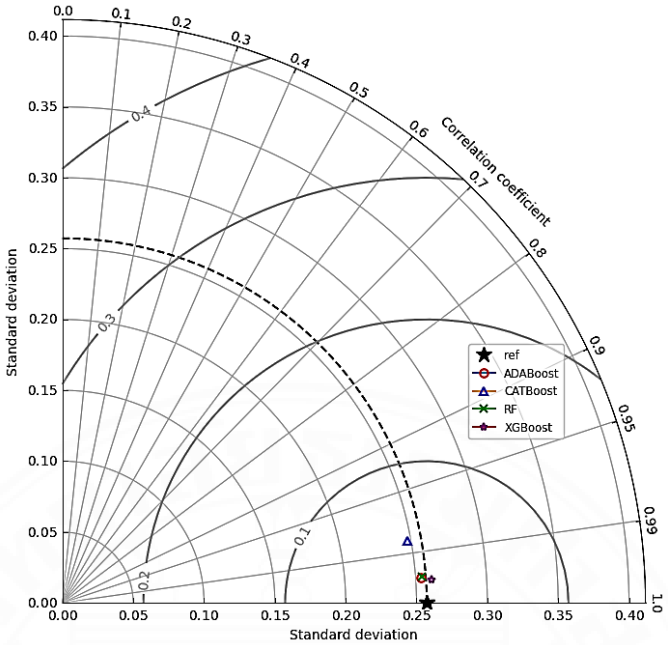

(b) Training phase.

Figure 4.8 Taylor diagram of *fy,T/fy* on post-fire steel test.

4.3 Rank Analysis

One technique for evaluating how well a model performed is rank analysis. Ranking analysis based on metric performance scores of data collected during the training and testing phases are used to create scores. A higher score indicates a greater relationship with a certain category, whereas a lower score may indicate uncertainty. The first place is assigned to the algorithm with the highest overall score, while the last belongs to the model with the lowest overall score. This method aids in evaluating the predictive ability of proposed algorithms. The rank analysis results for each of the models offered in this study are shown in Tables 4.8 to 4.11. Table 4.8 shows that the XGBoost approach performed better than the other models in forecasting the FRP-concrete pullout test, with a total potential score of 22. The CatBoost, XGBoost, and RF techniques had total scores of 20, 12, and 6, respectively. Table 4.9 shows that the AdaBoost approach performed better than the other models in forecasting the FRP-steel shear test, with a total potential score of 24. The XGBoost, CatBoost, and RF techniques had total scores of 18, 12, and 6, respectively. Table 4.10 shows that the AdaBoost approach performed better than the other models in forecasting the residual *fu,T/fu* of the steel test, with a total potential score of 23. The XGBoost, CatBoost and RF

techniques had total scores of 19, 12, and 6, respectively. Table 4.11 shows that the AdaBoost approach performed better than the other models in forecasting the residual *fy,T/fy* of the steel test, with a total potential score of 23. The XGBoost, RF, and CatBoost techniques had total scores of 17, 11, and 9, respectively.

Table 4.8 Rank analysis of FRP-concrete pull-out test.

Metric Performance		AdaBoost		CatBoost		XGBoost		RF	
		Train	Test	Train	Test	Train	Test	Train	Test
R^2	Value	0.9995	0.9994	0.9999	0.9957	1.0000	0.9993	1.0000	0.9991
	Score	1	4	2	1	4	3	3	2
RMSE	Value	0.0038	0.0044	0.0021	0.0119	0.0009	0.0049	0.0012	0.0056
	Score	1	4	2	1	4	3	3	2
MAE	Value	0.0009	0.0011	0.0016	0.0065	0.0006	0.0016	0.0003	0.0010
	Score	2	3	1	1	3	2	4	4
Subtotal score		4	11	5	3	11	8	10	8
Total score		15		8		19		18	
Rank		3rd		4th		1st		2nd	

Table 4.9 Rank analysis of FRP-steel shear test.

Metric Performance		AdaBoost		CatBoost		XGBoost		RF	
		Train	Test	Train	Test	Train	Test	Train	Test
R^2	Value	1	0.9988	0.99998	0.9887	0.99999	0.9986	0.9382	0.9401
	Score	4	4	2	2	3	3	1	1
RMSE	Value	0	0.0183	0.0020	0.050	0.0010	0.0189	0.0193	0.0177
	Score	4	4	2	2	3	3	1	1
MAE	Value	0	0.0067	0.0016	0.0275	0.0005	0.0072	0.0453	0.0410
	Score	4	4	2	2	3	3	1	1
Subtotal score		12	12	6	6	9	9	3	3
Total score		24		12		18		6	
Rank		1st		3rd		2nd		4th	

Table 4.10 Rank analysis of *fu,T/fu* post-fire steel test.

Metric Performance		AdaBoost		CatBoost		XGBoost		RF	
		Train	Test	Train	Test	Train	Test	Train	Test
R^2	Value	1	0.9986	0.99998	0.9826	0.99999	0.9991	0.9998	0.9617
	Score	4	3	2	2	3	4	1	1
RMSE	Value	0	0.0089	0.0010	0.0315	0.0005	0.0117	0.0034	0.0477
	Score	4	4	2	2	3	3	1	1
MAE	Value	0	0.0045	0.0008	0.0165	0.0003	0.0062	0.0013	0.0187
	Score	4	4	2	2	3	3	1	1
Subtotal score		12	12	11	6	6	9	10	3
Total score		23		12		19		6	
Rank		1st		3rd		2nd		4th	

Table 4.11 Rank analysis of *fy,T/fy* post-fire steel test.

Metric Performance		AdaBoost		CatBoost		XGBoost		RF	
		Train	Test	Train	Test	Train	Test	Train	Test
R^2	Value	1	0.9974	0.99995	0.9844	0.99999	0.9980	0.9998	0.9973
	Score	4	3	2	1	3	4	1	2
RMSE	Value	0	0.0133	0.0017	0.0329	0.0006	0.0140	0.0033	0.0134
	Score	4	4	2	1	3	2	1	3
MAE	Value	0	0.0047	0.0013	0.0193	0.0003	0.0070	0.0014	0.0049
	Score	4	4	2	1	3	2	1	3
Subtotal score		12	11	6	3	9	8	3	8
Total score		23		9		17		11	
Rank		1st		4th		2nd		3rd	

4.4 Sensitivity Analysis

4.4.1. Pearson correlation coefficient (PCC)

The PCC findings of each test are provided in Figures. 4.9 to Figure. 4.11. For the PCC of the concrete-FRP pull-out test parameters in Figure. 4.9, the d_b and l_b have a higher statistical connection with the output parameter (P_{max}), but the remaining variables have a weaker statistical connection. For the PCC of the steel-FRP shear test parameters in Figure. 4.10, E_A, f_A, t_A, and f_C indicate a nonlinear correlation with the output parameter (P_{max}), whereas the remaining variables (E_C, t_C, b_C, L_C) indicate a linear correlation with the output parameter (P_{max}). Figure 4.11 shows the PCC of the post-fire test parameters, The connection between *fu,T/fu* and thickness (mm) is linear, however, the relationship between temperature (°C) and *fu,T/fu* is nonlinear. However, thickness and *fy,T/fy* have a linear relationship based on the results of PCC

on forecasting *fy,T/fy*. Temperature (°C) and ultimate strength ratio *fy,T/fy* have a nonlinear relationship.

4.4.2. Feature importance (FI)

The FI findings of each test are provided in Figure 4.12 to Figure 4.14 for each test as the best overall performance model. Based on the result, the XGBoost is considered as the best forecasting technique in concrete-FRP pull-out test prediction. Figure 4.12 shows the parameter with the greatest impact on XGBoost output. embedment length (l_b) has the highest impact to the prediction with a value of 42.55%. Furthermore, the AdaBoost is considered as the best forecasting technique in steel-FRP shear test prediction. Figure 4.13 shows the FI value of the steel-FRP shear test, the parameter that has the greatest impact on output is CFRP thickness (t_C) with a value of 22.39%. Additionally, the AdaBoost technique is considered as the best forecasting technique in steel post-fire test prediction. Figure 4.14 shows the FI value of the steel post-fire test, the parameter that has the greatest impact on output, *fu,T/fu* and *fy,T/fy*, is temperature with a value of 75.42% and 76.03%, respectively.

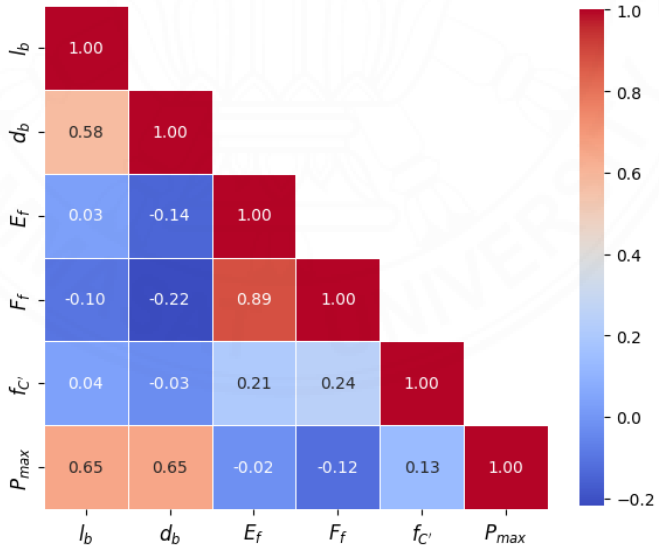

Figure 4.9 PCC of concrete-FRP pull-out test parameter.

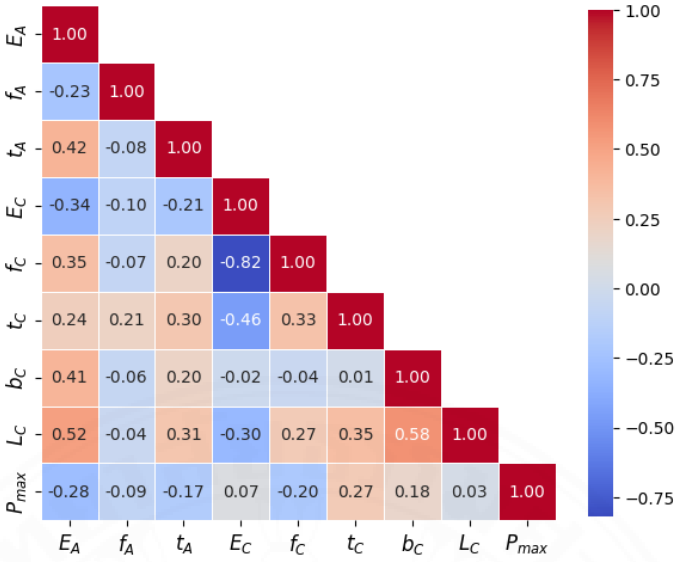

Figure 4.10 PCC of steel-FRP shear test parameter.

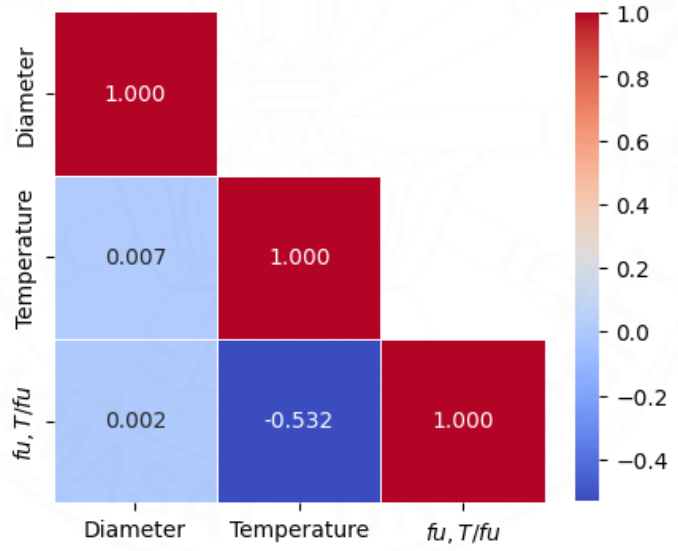

(a)

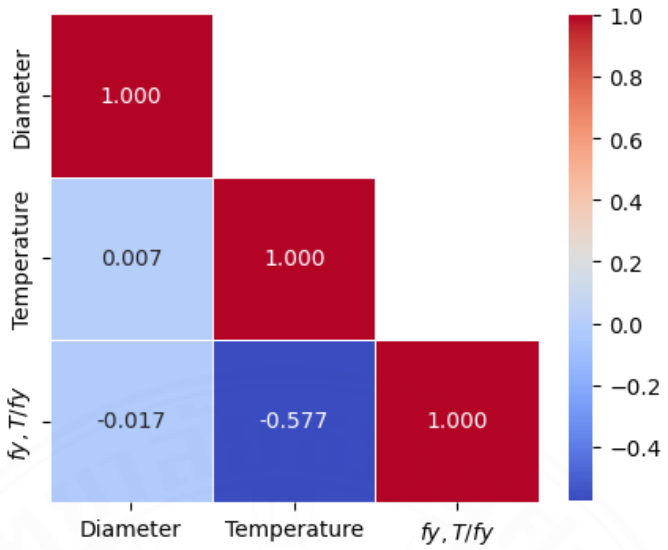

(b)

Figure 4.11 PCC of steel post-fire test parameters (a) ultimate strength ratio and (b) yield strength ratio.

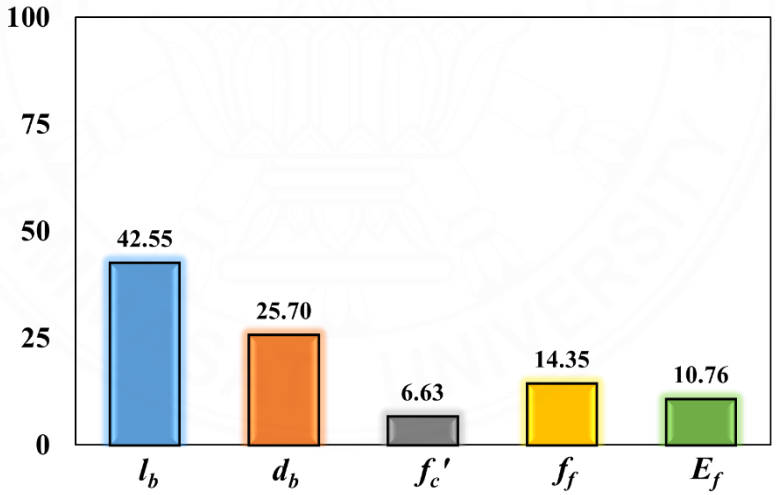

Figure 4.12 XGBoost FI of concrete-FRP pull-out test.

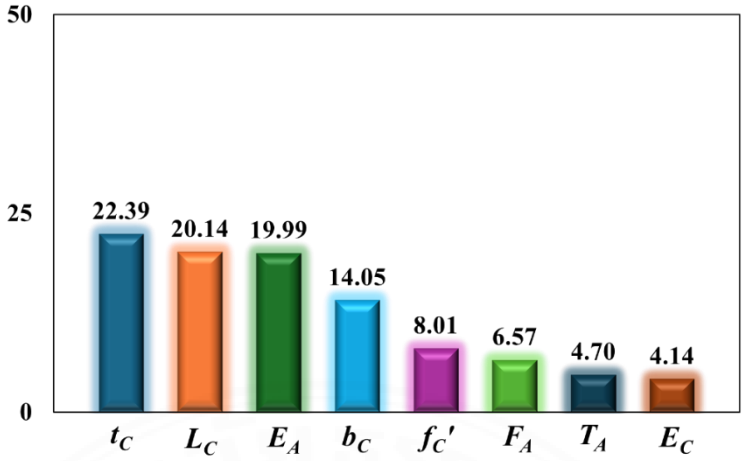

Figure 4.13 AdaBoost FI of the steel-FRP shear test.

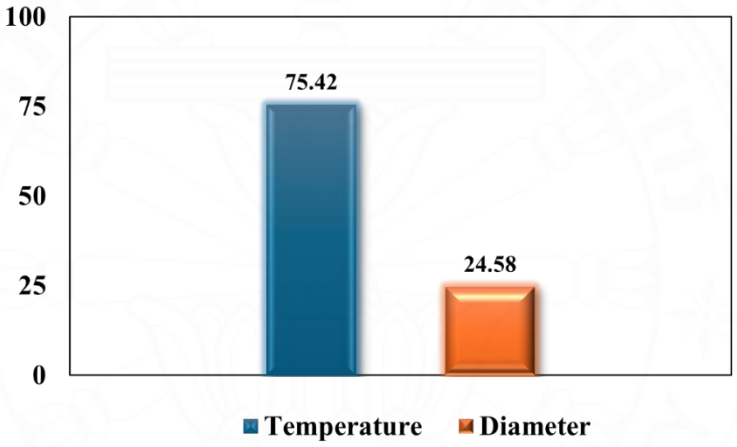

(a) FI of *fu,T/fu*.

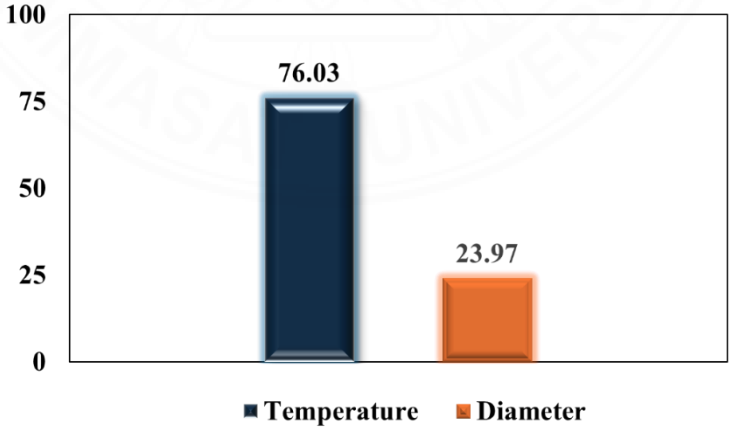

(b) FI of *fy,T/fy*.

Figure 4.14 AdaBoost FI of steel post-fire test.

CHAPTER 5
CONCLUSIONS AND RECOMMENDATIONS

5.1 Conclusions

5.1.1. Machine learning effectiveness models

This thesis study demonstrates the potential of advanced ensemble machine learning techniques (XGBoost, AdaBoost, CatBoost, and Random Forest) in accurately predicting critical material properties in civil engineering. The findings validate that these models can serve as robust tools for estimating the following:

1. Ultimate strength in FRP-concrete pull-out tests.
2. Ultimate shear stress at the FRP-steel interface during shear tests.
3. Residual ultimate strength (*fu,T/fu*) steel post-fire conditions.
4. Residual yield strength (*fy,T/fy*) steel post-fire conditions.

AdaBoost and XGBoost iterative boosting mechanism efficiently reduced errors. Its ability to adapt and learn from misclassified data allowed it to outperform other models, especially in datasets with moderate feature complexity and smaller sample sizes. The AdaBoost technique has the highest value score from rank analysis and shows the best scatter plot graph on each test including the training and testing phases in ultimate shear stress at the FRP-steel interface during shear tests and Residual mechanical properties of post-fire steel test. Additionally, the XGBoost technique has the highest value score from rank analysis in ultimate shear stress of FRP-concrete pull-out tests.

5.1.2. Data-driven insight of machine learning models

An analysis of feature importance revealed that bond length (l_b) was the most influential parameter for ultimate strength in FRP-concrete pull-out test setups, CFRP thickness (t_C) was the most influential parameter for ultimate shear stress at the FRP-steel interface during shear test setups, and temperature was the most influential parameter for residual ultimate strength (*fu,T/fu*) and residual yield strength (*fy,T/fy*) post-fire conditions setups. AdaBoost and XGBoost interpretability tools confirmed its

ability to provide not only accurate predictions but also actionable insights into the underlying relationships in the data.

5.2 Recommendations

Future studies should focus on enhancing model performance through advanced implementations, such as hybrid models, while expanding datasets and collecting more parameters for greater generalization. Practical use of this model could include creating easy-to-use software or online tools to help engineers make quick predictions. Using explainable AI methods like SHAP can make the model's predictions clearer and build trust in its results.

REFERENCES

Abuodeh, O. R., Abdalla, J. A., & Hawileh, R. A. (2020). Prediction of shear strength and behavior of RC beams strengthened with externally bonded FRP sheets using machine learning techniques. *Composite Structures*, *234*, 111698. https://doi.org/https://doi.org/10.1016/j.compstruct.2019.111698

Ahmad, M. S. (2017). Effect of sustained elevated temperature on mechanical behavior of reinforcing bar. *Procedia engineering*, *173*, 905-909. https://doi.org/https://doi.org/10.1016/j.proeng.2016.12.139

Alam, M., & Hussein, A. (2013). Size effect on shear strength of FRP reinforced concrete beams without stirrups. *Journal of composites for Construction*, *17*(4), 507-516. https://doi.org/https://doi.org/10.1061/(ASCE)CC.1943-5614.0000346

Altaee, M. J., Altayee, S. A., Kadhim, M. M., Jawdhari, A., Majdi, A., Chabuk, A., & Al-Ansari, N. (2022). Evaluation of Existing Bond-Slip Relations for CFRP-Steel Joints and New Model for Linear and Nonlinear Adhesives. *Advances in Civil Engineering*, *2022*(1), 3673438. https://doi.org/https://doi.org/10.1155/2022/3673438

Arrieta, A. B., Díaz-Rodríguez, N., Del Ser, J., Bennetot, A., Tabik, S., Barbado, A., García, S., Gil-López, S., Molina, D., & Benjamins, R. (2020). Explainable Artificial Intelligence (XAI): Concepts, taxonomies, opportunities and challenges toward responsible AI. *Information fusion*, *58*, 82-115. https://doi.org/https://doi.org/10.1016/j.inffus.2019.12.012

Baena, M., Torres, L., Turon, A., & Barris, C. (2009). Experimental study of bond behaviour between concrete and FRP bars using a pull-out test. *Composites Part B: Engineering*, *40*(8), 784-797. https://doi.org/https://doi.org/10.1016/j.compositesb.2009.07.003

Barkhordari, M. S., & Jawdhari, A. (2023). Machine learning based prediction model for plastic hinge length calculation of reinforced concrete structural walls. *Advances in Structural Engineering*, 13694332231174252. https://doi.org/https://doi.org/10.1177/13694332231174252

Basaran, B., Kalkan, I., Bergil, E., & Erdal, E. (2021). Estimation of the FRP-concrete bond strength with code formulations and machine learning algorithms. *Composite Structures*, *268*, 113972. https://doi.org/https://doi.org/10.1016/j.compstruct.2021.113972

Başaran, B., Kalkan, İ., Beycioğlu, A., & Kasprzyk, I. (2022). A review on the physical parameters affecting the bond behavior of FRP bars embedded in concrete. *Polymers*, *14*(9), 1796. https://doi.org/https://doi.org/10.3390/polym14091796

Breiman, L. (2001). Random forests. *Machine learning*, *45*, 5-32. https://doi.org/https://doi.org/10.1023/A:1010933404324

Chen, J., Young, B., & Uy, B. (2006). Behavior of high strength structural steel at elevated temperatures. *Journal of Structural Engineering*, *132*(12), 1948-1954. https://doi.org/https://doi.org/10.1061/(ASCE)0733-9445(2006)132:12(1948)

Chen, L., Liang, K., & Shan, Z. (2023). Experimental and theoretical studies on bond behavior between concrete and FRP bars with different surface conditions. *Composite Structures*, *309*, 116721. https://doi.org/https://doi.org/10.1016/j.compstruct.2023.116721

Chiew, S., Zhao, M., & Lee, C. (2014). Mechanical properties of heat-treated high strength steel under fire/post-fire conditions. *Journal of Constructional Steel Research*, *98*, 12-19. https://doi.org/https://doi.org/10.1016/j.jcsr.2014.02.003

El Refai, A., Ammar, M.-A., & Masmoudi, R. (2015). Bond performance of basalt fiber-reinforced polymer bars to concrete. *Journal of composites for Construction*, *19*(3), 04014050. https://doi.org/https://doi.org/10.1061/(ASCE)CC.1943-5614.0000487

Elghazouli, A., Cashell, K., & Izzuddin, B. (2009). Experimental evaluation of the mechanical properties of steel reinforcement at elevated temperature. *Fire Safety Journal*, *44*(6), 909-919. https://doi.org/https://doi.org/10.1016/j.firesaf.2009.05.004

En, B. (2001). 10002-1: 2001. Tensile testing of metallic materials. Method of test at ambient temperature. *British Standards Institution*.

Fan, S., Ding, X., Sun, W., Zhang, L., & Liu, M. (2016). Experimental investigation on fire resistance of stainless steel columns with square hollow section. *Thin-Walled Structures*, *98*, 196-211. https://doi.org/https://doi.org/10.1016/j.tws.2015.02.003

Felicetti, R., Gambarova, P. G., & Meda, A. (2009). Residual behavior of steel rebars and R/C sections after a fire. *Construction and building materials*, *23*(12), 3546-3555. https://doi.org/https://doi.org/10.1016/j.conbuildmat.2009.06.050

Fernando, N. D. (2010). Bond behaviour and debonding failures in CFRP-strengthened steel members.

Godat, A., Aldaweela, S., Aljaberi, H., Al Tamimi, N., & Alghafri, E. (2021). Bond strength of FRP bars in recycled-aggregate concrete. *Construction and building materials*, *267*, 120919. https://doi.org/https://doi.org/10.1016/j.conbuildmat.2020.120919

He, J., & Xian, G. (2016). Debonding of CFRP-to-steel joints with CFRP delamination. *Composite Structures*, *153*, 12-20. https://doi.org/https://doi.org/10.1016/j.compstruct.2016.05.100

Hossain, K. M. A., Ametrano, D., & Lachemi, M. (2018). The bond between glass-fibre-reinforced polymer bars and ultra-high-strength concrete. *Proceedings of the Institution of Civil Engineers-Construction Materials*, *171*(4), 161-176. https://doi.org/https://doi.org/10.1680/jcoma.16.00032

Huang, G., Wu, L., Ma, X., Zhang, W., Fan, J., Yu, X., Zeng, W., & Zhou, H. (2019). Evaluation of CatBoost method for prediction of reference evapotranspiration in humid regions. *Journal of Hydrology*, *574*, 1029-1041. https://doi.org/https://doi.org/10.1016/j.jhydrol.2019.04.085

Irshidat, M. R. (2020). Improved bond behavior between FRP reinforcing bars and concrete with carbon nanotubes. *Construction and building materials*, *257*, 119562. https://doi.org/https://doi.org/10.1016/j.conbuildmat.2020.119562

Jacintho, A., Silva, V., Requena, J., Lintz, R., Barbosa, L., & Pimentel, L. (2012). Short steel and concrete columns under high temperatures. *Revista IBRACON*

de Estruturas e Materiais, *5*, 530-547. https://doi.org/https://doi.org/10.1590/S1983-41952012000400007

Kim, B., Lee, D.-E., Hu, G., Natarajan, Y., Preethaa, S., & Rathinakumar, A. P. (2022). Ensemble machine learning-based approach for predicting of FRP–concrete interfacial bonding. *Mathematics*, *10*(2), 231. https://doi.org/https://doi.org/10.3390/math10020231

Kodur, V., Dwaikat, M., & Fike, R. (2010). High-temperature properties of steel for fire resistance modeling of structures. *Journal of Materials in Civil Engineering*, *22*(5), 423-434. https://doi.org/https://doi.org/10.1061/(ASCE)MT.1943-5533.0000041

Kumar, W., Sharma, U. K., & Shome, M. (2021). Mechanical properties of conventional structural steel and fire-resistant steel at elevated temperatures. *Journal of Constructional Steel Research*, *181*, 106615. https://doi.org/https://doi.org/10.1016/j.jcsr.2021.106615

Lee, G. C., Mohan, S., Huang, C., & Fard, B. N. (2013). *A study of US bridge failures (1980-2012)*. MCEER Buffalo, NY.

Li, G.-Q., Jiang, S.-C., Yin, Y.-Z., Chen, K., & Li, M.-F. (2003). Experimental studies on the properties of constructional steel at elevated temperatures. *Journal of Structural Engineering*, *129*(12), 1717-1721. https://doi.org/https://doi.org/10.1061/(ASCE)0733-9445(2003)129:12(1717)

Liang, K., Chen, L., Shan, Z., & Su, R. (2023). Experimental and theoretical study on bond behavior of helically wound FRP bars with different rib geometry embedded in ultra-high-performance concrete. *Engineering Structures*, *281*, 115769. https://doi.org/https://doi.org/10.1016/j.engstruct.2023.115769

Maraveas, C., Fasoulakis, Z. C., & Tsavdaridis, K. D. (2017). Mechanical properties of high and very high steel at elevated temperatures and after cooling down. *Fire Science Reviews*, *6*, 1-13. https://doi.org/https://doi.org/10.1186/s40038-017-0017-6

Nepomuceno, E., Sena-Cruz, J., Correia, L., & D'Antino, T. (2021). Review on the bond behavior and durability of FRP bars to concrete. *Construction and building materials*, *287*, 123042. https://doi.org/https://doi.org/10.1016/j.conbuildmat.2021.123042

Ou, J., Shao, Y., Huang, C., & Bi, X. (2023). Bond behavior of CFRP sheets-to-steel shear joints with different steel surface treatments. *Composite Structures*, *322*, 117376. https://doi.org/https://doi.org/10.1016/j.compstruct.2023.117376

Pang, Y.-Y., Wu, G., Wang, H.-T., Su, Z.-L., & He, X.-Y. (2020). Experimental study on the bond behavior of the CFRP-steel interface under the freeze–thaw cycles. *Journal of Composite Materials*, *54*(1), 13-29. https://doi.org/https://doi.org/10.1177/0021998319851191

Peng, K.-D., Zeng, J.-J., Huang, B.-T., Huang, J.-Q., Zhuge, Y., & Dai, J.-G. (2022). Bond performance of FRP bars in plain and fiber-reinforced geopolymer under pull-out loading. *Journal of Building Engineering*, *57*, 104893. https://doi.org/https://doi.org/10.1016/j.jobe.2022.104893

Rahman, H. A. A., Wah, Y. B., He, H., & Bulgiba, A. (2015). Comparisons of ADABOOST, KNN, SVM and logistic regression in classification of imbalanced dataset. Soft Computing in Data Science: First International

Conference, SCDS 2015, Putrajaya, Malaysia, September 2-3, 2015, Proceedings 1,

Rengasamy, D., Mase, J. M., Kumar, A., Rothwell, B., Torres, M. T., Alexander, M. R., Winkler, D. A., & Figueredo, G. P. (2022). Feature importance in machine learning models: A fuzzy information fusion approach. *Neurocomputing*, *511*, 163-174. https://doi.org/https://doi.org/10.1016/j.neucom.2022.09.053

Rolland, A., Quiertant, M., Khadour, A., Chataigner, S., Benzarti, K., & Argoul, P. (2018). Experimental investigations on the bond behavior between concrete and FRP reinforcing bars. *Construction and building materials*, *173*, 136-148. https://doi.org/https://doi.org/10.1016/j.conbuildmat.2018.03.169

Saleh, N., Ashour, A., Lam, D., & Sheehan, T. (2019). Experimental investigation of bond behaviour of two common GFRP bar types in high–Strength concrete. *Construction and building materials*, *201*, 610-622. https://doi.org/https://doi.org/10.1016/j.conbuildmat.2018.12.175

Samad, A. A. A., Mohamad, N., Ali, N., Jayaprakash, J., & Mendis, P. (2016). Rehabilitation of continuous reinforced concrete beams in shear by external bonding of carbon fiber reinforced polymer strips for sustainable construction. *Key Engineering Materials*, *708*, 49-58. https://doi.org/https://doi.org/10.4028/www.scientific.net/KEM.708.49

Shan, Z., Liang, K., & Chen, L. (2023). Bond behavior of helically wound FRP bars with different surface characteristics in fiber-reinforced concrete. *Journal of Building Engineering*, *65*, 105504. https://doi.org/https://doi.org/10.1016/j.jobe.2022.105504

Su, M., Peng, H., Yuan, M., & Li, S. (2021). Identification of the interfacial cohesive law parameters of FRP strips externally bonded to concrete using machine learning techniques. *Engineering Fracture Mechanics*, *247*, 107643. https://doi.org/https://doi.org/10.1016/j.engfracmech.2021.107643

Su, M., Zhong, Q., Peng, H., & Li, S. (2021). Selected machine learning approaches for predicting the interfacial bond strength between FRPs and concrete. *Construction and building materials*, *270*, 121456. https://doi.org/https://doi.org/10.1016/j.conbuildmat.2020.121456

Sulayman, Q. A., & Mahmood, M. (2021). Post-fire performance of structural steel. *Diyala Journal of Engineering Sciences*, 28-41. https://doi.org/https://doi.org/10.24237/djes.2021.14203

Sundarraja, M., & Rajamohan, S. (2009). Strengthening of RC beams in shear using GFRP inclined strips–An experimental study. *Construction and building materials*, *23*(2), 856-864. https://doi.org/https://doi.org/10.1016/j.conbuildmat.2008.04.008

Tariq, F., & Bhargava, P. (2018). Residual mechanical behavior of (SD 500) hot rolled TMT reinforcing steel bars after elevated temperatures. *Construction and building materials*, *190*, 551-559. https://doi.org/https://doi.org/10.1016/j.conbuildmat.2018.09.008

Taylor, K. E. (2001). Summarizing multiple aspects of model performance in a single diagram. *Journal of geophysical research: atmospheres*, *106*(D7), 7183-7192. https://doi.org/https://doi.org/10.1029/2000JD900719

Ünlüoğlu, E., Topçu, İ. B., & Yalaman, B. (2007). Concrete cover effect on reinforced concrete bars exposed to high temperatures. *Construction and*

building materials, *21*(6), 1155-1160. https://doi.org/https://doi.org/10.1016/j.conbuildmat.2006.11.019

Usmani, A. S., Chung, Y., & Torero, J. L. (2003). How did the WTC towers collapse: a new theory. *Fire Safety Journal*, *38*(6), 501-533. https://doi.org/https://doi.org/10.1016/S0379-7112(03)00069-9

Wang, H.-T., Liu, S.-S., Liu, Q.-L., Pang, Y.-Y., & Shi, J.-W. (2021). Influences of the joint and epoxy adhesive type on the CFRP-steel interfacial behavior. *Journal of Building Engineering*, *43*, 103167. https://doi.org/https://doi.org/10.1016/j.jobe.2021.103167

Wang, H.-T., & Wu, G. (2018). Bond-slip models for CFRP plates externally bonded to steel substrates. *Composite Structures*, *184*, 1204-1214. https://doi.org/https://doi.org/10.1016/j.compstruct.2017.10.033

Wang, H.-T., Wu, G., Dai, Y.-T., & He, X.-Y. (2016a). Determination of the bond–slip behavior of CFRP-to-steel bonded interfaces using digital image correlation. *Journal of Reinforced Plastics and Composites*, *35*(18), 1353-1367. https://doi.org/https://doi.org/10.1177/0731684416651342

Wang, H.-T., Wu, G., Dai, Y.-T., & He, X.-Y. (2016b). Experimental study on bond behavior between CFRP plates and steel substrates using digital image correlation. *Journal of composites for Construction*, *20*(6), 04016054. https://doi.org/https://doi.org/10.1061/(ASCE)CC.1943-5614.0000701

Wang, W.-C., Nguyen, N.-M., & Cao, M.-T. (2022). Smart ensemble machine learner with hyperparameter-free for predicting bond capacity of FRP-to-concrete interface: Multi-national data. *Construction and building materials*, *345*, 128158. https://doi.org/https://doi.org/10.1016/j.conbuildmat.2022.128158

Wang, W.-y., Liu, B., & Kodur, V. (2013). Effect of temperature on strength and elastic modulus of high-strength steel. *Journal of Materials in Civil Engineering*, *25*(2), 174-182. https://doi.org/https://doi.org/10.1061/(ASCE)MT.1943-5533.0000600

Wang, X.-Q., Tao, Z., & Hassan, M. K. (2020). Post-fire behaviour of high-strength quenched and tempered steel under various heating conditions. *Journal of Constructional Steel Research*, *164*, 105785. https://doi.org/https://doi.org/10.1016/j.jcsr.2019.105785

Wang, Z., Li, C., Sui, L., & Xian, G. (2021). Effects of adhesive property and thickness on the bond performance between carbon fiber reinforced polymer laminate and steel. *Thin-Walled Structures*, *158*, 107176. https://doi.org/https://doi.org/10.1016/j.tws.2020.107176

Wu, C., Zhao, X., Duan, W. H., & Al-Mahaidi, R. (2012). Bond characteristics between ultra high modulus CFRP laminates and steel. *Thin-Walled Structures*, *51*, 147-157. https://doi.org/https://doi.org/10.1016/j.tws.2011.10.010

Yu, T., Fernando, D., Teng, J., & Zhao, X. L. (2012). Experimental study on CFRP-to-steel bonded interfaces. *Composites Part B: Engineering*, *43*(5), 2279-2289. https://doi.org/https://doi.org/10.1016/j.compositesb.2012.01.024

Yuan, C., He, C., Xu, J., Liao, L., & Kong, Q. (2022). Bayesian optimization for selecting efficient machine learning regressors to determine bond-slip model of FRP-to-concrete interface. Structures,

Zhang, F., Wang, C., Liu, J., Zou, X., Sneed, L. H., Bao, Y., & Wang, L. (2023). Prediction of FRP-concrete interfacial bond strength based on machine learning. *Engineering Structures*, *274*, 115156. https://doi.org/https://doi.org/10.1016/j.engstruct.2022.115156

Zhang, R., & Xue, X. (2021). A predictive model for the bond strength of near-surface-mounted FRP bonded to concrete. *Composite Structures*, *262*, 113618. https://doi.org/https://doi.org/10.1016/j.compstruct.2021.113618

Zhang, S.-Y., Chen, S.-Z., Jiang, X., & Han, W.-S. (2022). Data-driven prediction of FRP strengthened reinforced concrete beam capacity based on interpretable ensemble learning algorithms. Structures,

Zhao, X.-L., & Zhang, L. (2007). State-of-the-art review on FRP strengthened steel structures. *Engineering Structures*, *29*(8), 1808-1823. https://doi.org/https://doi.org/10.1016/j.engstruct.2006.10.006

Zhou, W., Feng, P., Lin, H., & Zhou, P. (2023). Bond behavior between GFRP bars and coral aggregate concrete. *Composite Structures*, *306*, 116567. https://doi.org/https://doi.org/10.1016/j.compstruct.2022.116567

Zhou, Y., Wu, G., Li, L., Guan, Z., Guo, M., Yang, L., & Li, Z. (2022). Experimental investigations on bond behavior between FRP bars and advanced sustainable concrete. *Polymers*, *14*(6), 1132. https://doi.org/https://doi.org/10.3390/polym14061132

Zhou, Y., Zheng, S., Huang, Z., Sui, L., & Chen, Y. (2020). Explicit neural network model for predicting FRP-concrete interfacial bond strength based on a large database. *Composite Structures*, *240*, 111998. https://doi.org/https://doi.org/10.1016/j.compstruct.2020.111998

BIOGRAPHY

Name	Irwan Afriadi
Educational Attainment	Academic Year 2023: Master of Civil Engineering. Thammasat School of Engineering. Thammasat University. Thailand
Scholarship (If any)	Year 2023: Thammasat International Scholarship Recruitment (TISR)